7-26

SANDIA REPORT

SAND95-1472 • UC-703
Unlimited Release
Printed July 1995

Measuring the Dynamic Compression and Release Behavior of Rocks Associated with HYDROPLUS (Part II)

Michael D. Furnish

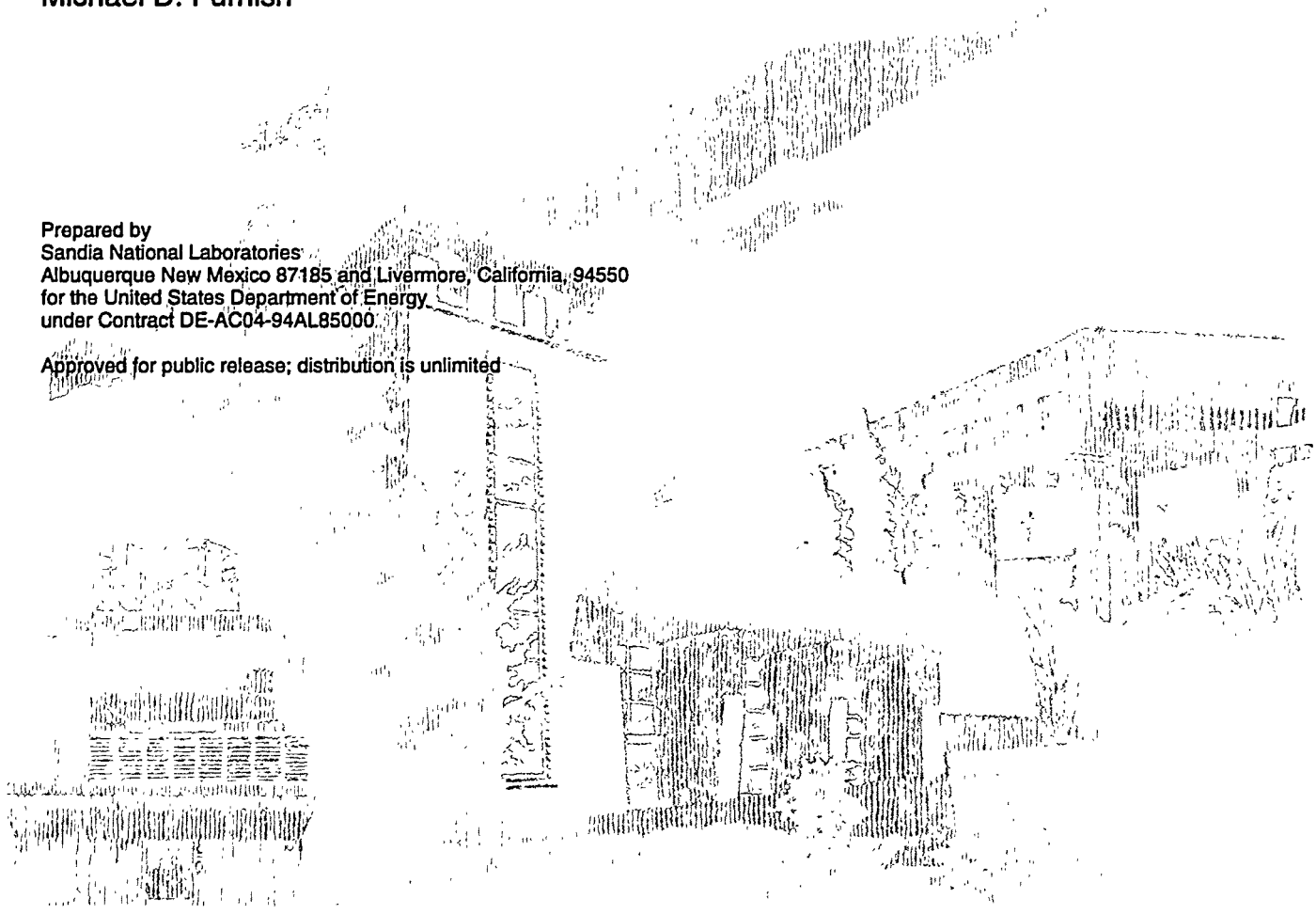

Prepared by
Sandia National Laboratories
Albuquerque New Mexico 87185 and Livermore, California, 94550
for the United States Department of Energy
under Contract DE-AC04-94AL85000

Approved for public release; distribution is unlimited

Issued by Sandia National Laboratories, operated for the United States Department of Energy by Sandia Corporation

Available to DOE and DOE contractors from
Office of Scientific and Technical Information
PO Box 62
Oak Ridge, TN 37831
Prices available from (615) 576-8401

Available to the public from
National Technical Information Service
US Department of Commerce
5285 Royal Port Rd
Springfield, VA 22161
NTIS price codes
Printed copy: A04
Microfiche copy: A01

SAND95-1472
Unlimited Release
Printed July 1995

Distribution
Category UC-703

Measuring the Dynamic Compression and Release Behavior of Rocks Associated with HYDROPLUS (Part II)

Michael D. Furnish
Experimental Impact Physics Department
Sandia National Laboratories
Albuquerque NM 87185

Abstract

Three sets of rock samples have been subjected to planar impact to characterize loading, Hugoniot and release responses. A slate from Pennsylvania was tested over the stress range of 5 GPa to 140 GPa. Phyllite from the Lupin Mine (Canada) was tested over the 14 - 50 GPa stress region. Finally, granite samples from the SHIST test site (New Mexico) were tested over the 10 - 20 GPa stress region. The granite tests included a transmitted-wave experiment at about 10 GPa. In 12 of the 13 tests, a reverse-ballistic configuration (optimized for Hugoniot and release measurements) was used. The remaining test (conducted on the granite) provided a transmitted waveform from which precursor, Hugoniot and release properties were obtained. Velocity interferometry (VISAR) was used as the primary diagnostic throughout. The slate data showed an unexpected inflection downward in the Hugoniot at around 8 GPa. The slate and granite showed release paths lying below the Hugoniot for lower stress levels (below ~60 GPa), while the slate release paths were "normal" (above the Hugoniot) at higher stress levels. In addition, the granite releases were found to lie substantially below the Hugoniot in the 30 - 40 GPa region; this may be related to the quartz-stishovite transition. The present results are generally consistent with earlier work.

Acknowledgments

I would like to acknowledge the help from the technicians at the STAR Facility, especially Ron McIntosh, who performed the majority of the sometimes enjoyable, sometimes onerous or tedious chores of preparing and firing the shots. I also appreciate the participation of Audrey Martinez of FCDNA, who created a team which genuinely felt like a team, including the Ktech gas-gun experts and myself. This is more than the description of a contract monitor requires, which does not include "participation." Tom Bergstresser, Mark Boslough and Paul Yarrington marked up ~~final~~ draft versions, and their much-appreciated reviews [forced me to] greatly improve[d] the readability of this report. Finally (obligatory statement, happily recorded) I acknowledge the support of my wife and family in doing this work.

Table of Contents

Figures

Tables

This page intentionally left blank

Measuring the Dynamic Compression and Release Behavior of Rocks Associated with HYDROPLUS (Part II)

1.0 Introduction and Technique

This report is intended as a follow-on to an earlier report [Furnish, 1993a], discussing analogous measurements performed on a variety of tuffs, rhyolites, carbonates, grouts, as well as a quartzite permafrost and an epoxy-alumina gauge potting material. That document presented a detailed discussion of experimental method, so only a brief summary of the method will be included here.

1.1 Motivation

These tests were conducted in support of the Defense Nuclear Agency HYDROPLUS project, whose aim is to measure the yield of underground nuclear tests by means of near-field particle velocity and stress gauges. Alternative means of performing such measurements include CORRTEX (a wave-velocity diagnostic) and far-field seismic measurements. The end goal of such measurements is to ensure compliance of the testing party with the 1974 Threshold Test Ban Treaty, which limits yields to 150 kilotons, while adhering to the 1990 Protocols [USACDA/USOSIA, 1990]. The Protocols impose a large number of restrictions on the verification method; much of the effort of the HYDROPLUS program has been to satisfy those restrictions while making a credible yield measurement.

Important to such a yield measurement is an assessment of the dynamic loading and release properties of the country rock near a test, as well as of gauge emplacement grouts. These measurements are then used to constrain computations of the groundshock, which are compared to observed values to determine the yield.

Three rock materials were studied in the present portion of the Sandia effort supporting HYDROPLUS, generally in a reverse-ballistic configuration which is optimized for Hugoniot and release property measurement (see Section 1.2). Slate from Pennsylvania was tested over the stress range of 5 GPa to 140 GPa. Phyllite from the Lupin Mine (Canada) was tested over the 14 - 50 GPa stress region. Finally, granite samples from the SHIST test site (New Mexico) were tested over the 10 - 20 GPa stress region, including a transmitted-wave experiment at about 10 GPa.

1.2 Experimental techniques

The present section contains a brief review of the experimental techniques used for dynamic materials properties measurements on rock materials. It is included to make this

report self-contained. More detailed discussions of wave interactions, data reduction methods and uncertainties may be found in Furnish [1993a, b] and Grady and Furnish [1988]. Details of data reduction methods will be presented where appropriate in the remainder of this report.

1.2.1 Considerations for impact studies of geological materials

The impact characterization of geological materials poses special challenges. Most importantly, samples are likely to contain heterogeneities (mm or larger scale). These affect experiments in several ways. Often a buffer must be used between the sample and the gauge or reflecting surface to protect it from the effects of an uneven shock, as well as to average a signal passed through the heterogeneous sample. On the other hand, buffers inevitably perform some shock processing, so it is preferable to eliminate them if possible. Samples must be selected with an eye toward having results represent the bulk of the available material, but at the same time the samples must be uniform enough to allow a meaningful experiment (restrictions which may be difficult to satisfy simultaneously). Sample selection generally favors the most homogeneous and competent samples, and as such may bias the results of any dynamic study of these materials in that direction.

The effects of heterogeneities are more important at lower pressures. As interest shifts from groundshock behavior at high stress levels ($\sigma > 10$ GPa) to groundshock behavior in the stress region only slightly above the elastic limit ($\sigma \sim 0.1$ GPa), both small-scale inhomogeneities such as selectively altered crystals and large-scale inhomogeneities such as joint systems become important. In the present study, the majority of the tests were conducted at stress levels above 10 GPa. Related tests (e.g. Gaffney and Smith [1994]) were conducted primarily at low enough stress levels that this was an issue.

Often water is an important component of the material of interest. When it is, the experiment may need to isolate the sample from vacuum, and possibly from gauges or reflective films as well. The sample may need to be machined without being allowed to dry. If the sample location is above the water table, the sample may be partially saturated. Such partial saturations are extremely difficult to maintain, and the only practical avenue may be to choose an end-member saturation for the tests. The samples in the present study, presumed to have extremely low porosity, were exposed to room air and the vacuum in the gun system. The effect of this potential drying was minor; the weight change of a sample of slate subjected to vacuum for 30 minutes was negligible (see Section 2.2).

Final, the sample may be friable or cracked. Such a sample may not machine well, or may require containment to withstand the kilogravity to megagravity environment of a gun launch without damage. The 1990 Protocols do not allow a large amount of rock sampling, so a team performing gas gun testing may be required to use some imperfect samples.

1.2.2 Experimental configurations of interest

Forward ballistic (transmitted wave) configuration

In the most generally usable configuration for gas-gun testing, the sample is placed in the

target (Figure 1-1). This configuration is especially appropriate for measuring loading wave profiles, Hugoniot states and strength properties (Hugoniot Elastic Limit for loading, the strength at the Hugoniot state, and the tensile or spall strength). If a window material can be chosen which is an approximate shock impedance match for the sample (such as Z-cut sapphire for iron, or lithium fluoride for slate or granite), a continuous release path can be measured; otherwise the pressure and particle velocity of a single point on the release (or reshock) path of the sample can be determined. If a window material is chosen which has a much lower shock impedance than does the sample, spall properties of the sample can be measured as well as Hugoniot properties.

Analysis of the velocity profile from such a test consists of determining the precursor and

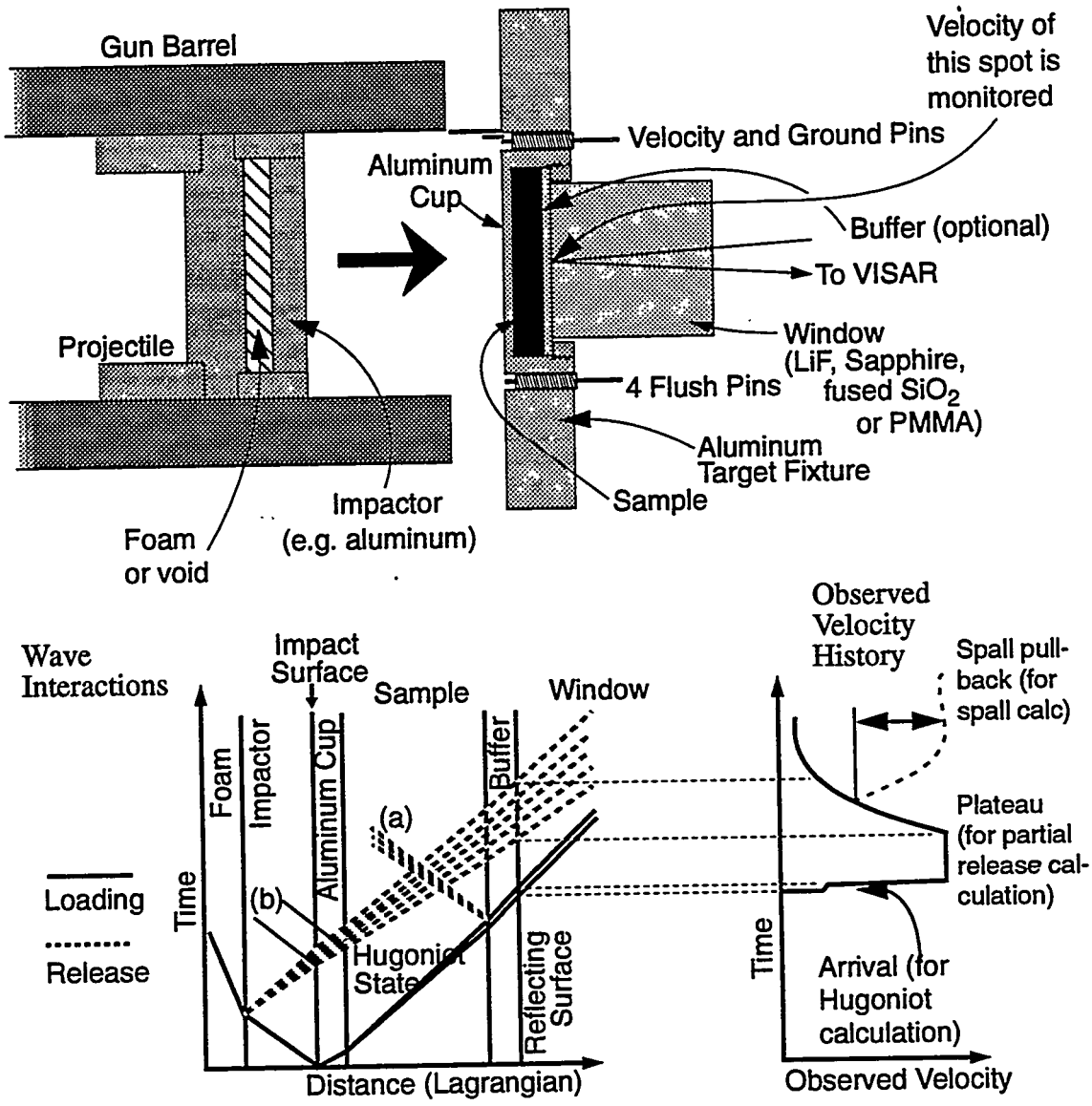

Figure 1-1. Forward ballistic configuration (a) Release or reshock from sample/buffer interface; (b) Reshock from sample/cup interface (and cup/impactor for non-aluminum impactor)

Hugoniot states from the transit time across the sample (hence velocity of the observed waves), then extracting available release or spall information [Furnish, 1993a]. If the window is a fairly close impedance match to the sample and the waveforms entering and leaving the sample are known (easiest if no buffer is used), Lagrangian integration of the wave velocities yields a table relating stress, strain, time, shock velocity and wave velocity [Furnish, 1992]. For many materials, the strain rate during loading varies approximately as the fourth power of the Hugoniot stress [Swegle and Grady, 1985]. If buffers are used, wavecode modeling of the experiment to match the observed waveform may yield the pressure-volume path, although this procedure is somewhat more laborious. If the window is a poor impedance match for the sample, the average amplitude of the waveform "plateau" may be used with the Hugoniot of the window to calculate a single partial release or reshock state of the sample. Finally, if the sample has spalled, the amplitude of the pull-back signal may yield the spall strength of the sample [Chhabildas, et al, 1990].

Reverse ballistic configuration

For conditions where a window whose shock impedance matches the shock impedance of the sample cannot be found, Hugoniot and continuous release paths can be measured using the geometry shown in Figure 1-2. Wave interactions and a typical velocity history are indicated. This configuration, called "reverse-ballistic," has been used extensively for measuring Hugoniot and release properties of rocks and grouts. It can be used with water-saturated samples (as can the forward-ballistic configuration). It does not give any information about loading characteristics, such as precursors and material strength, and in fact can give erroneous Hugoniot density and shock velocity values if incorrect assumptions about precursors are made [Furnish, 1993a]. It is normally most useful if the dynamic strength of the material is small compared to the Hugoniot stress.

1.2.3 Strengths and limitations of gun impact tests for EOS measurements

Let us make several general comments about planar impact tests (generally performed on precision gun systems, and hence referred to as "gun impact tests"). Fundamentally these tests are uniaxial tests of hand-specimen-sized samples. This raises two issues.

First, because of sample size limitations, such tests cannot readily assess large-scale properties of heterogeneous bodies. Various studies have been performed to assess the roles of heterogeneities, generally aimed to model or observe a system with one or a few simple structures, although the behavior of families of these features under high strain rates remains unclear (but of considerable importance for stresses near the elastic limit of these materials).

Second, the present experiments are designed to measure only the uniaxial strain properties of samples. Wave divergence phenomena are found near the margins of samples in planar impact tests. If such phenomena are of interest, however, the more traditional divergent wave experiments (exploding wire or point charge) can allow a more straightforward relation to physical systems of interest.

On the other hand, gas-gun tests conducted to separate shear and longitudinal properties

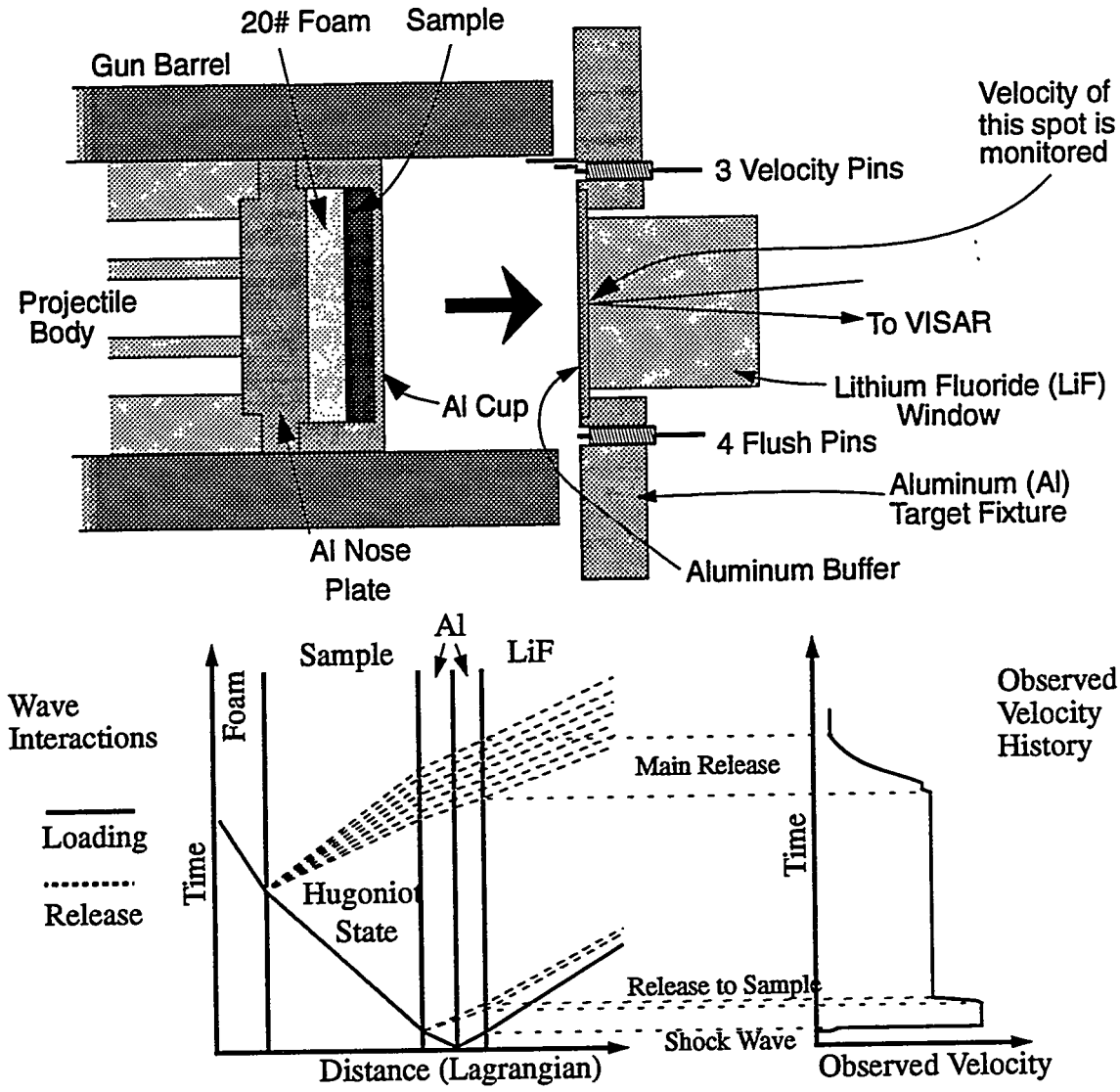

Figure 1-2. Reverse ballistic configuration

can be useful experiments for benchmarking individual parameters in material models for calculating nonplanar wave behavior. These tests normally require generating a plane shear wave by a tilt-impact or anisotropic shock-processing material (e.g. Y-cut quartz), then coupling this wave from the impactor or buffer into the sample and from the sample into the window. For geologic materials, this coupling is difficult and hard to ascertain. When such experiments can be made to work, they can constrain a large set of physical parameters describing the dynamic behavior of the material [Aidun and Gupta, 1989]. They are able, as well, to separate volume effects (such as phase transitions) from strength- and Poisson's ratio- effects such as the Hugoniot elastic limit and strength effects upon release. These effects generally cannot be separated in a simple longitudinal wave impact experiment.

Various window materials remain transparent over different stress ranges. The most common window materials in use, and their useful upper stress limits, are lithium fluoride (160

GPa +) [Wise and Chhabildas, 1985], Z-cut sapphire (elastic to 14 GPa; may recover transparency above 50 - 60 GPa) [Barker and Hollenbach, 1970], PMMA (20 GPa; has viscoelastic behavior) [Schuler and Nunziato, 1975], and fused silica (8 GPa; produces ramp wave below 3 GPa) [Barker and Hollenbach, 1970]. At low stress ranges (1 - 3 GPa), lithium fluoride is slightly affected by its elastic-plastic transition. Within these constraints, gas gun tests are able to produce a wide range of materials properties data for materials undergoing high strain-rate deformation.

In summary, the waveform shown in Figure 1-3 illustrates representative properties which can be obtained for metallic or stony geological materials (represented here for a forward-ballistic test).

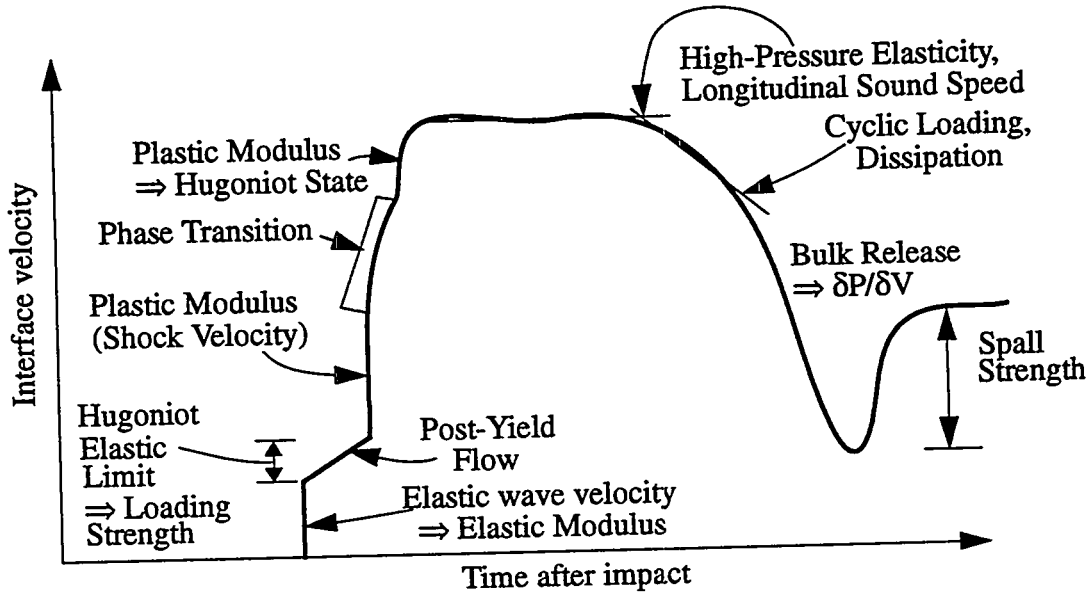

Figure 1-3. Correspondence between wave features and physical properties for a forward-ballistic (transmitted wave) experiment.

2.0 Impact Tests on Pennsylvania Slate

2.1 Materials studied

Blocks of competent slate were obtained from a quarry approximately 14 miles north-northwest of Allentown, Pennsylvania [Meyers, 1992] in November of 1992. This slate is quarried from the Ordovician-age Martinsburg Formation. Seven blocks (approx. 125 × 125 × 65 mm in size) were obtained for use in HYDROPLUS testing. Five of these samples (designated S-3 through S-7) had been protected from freezing by storage in the mill building at the quarry, while the other two (S-1 and S-2) had been stored outside and subjected to freezing since excavation. Samples S-1 and S-2 were not used in this study.

Blocks S-3, 4 and 5 were chosen for impact testing (S-5 at Sandia and S-3 and S-4 at the DNA Impact Facility). These had been cut from a single larger block, so the results of the Sandia tests should be relatable to physical properties results from Terra Tek [Martin, 1993] (from Sample S-3) and to wave profile data from the DNA facility [Davies and Smith, 1994]. No attempts were made to maintain water saturation or to desiccate.

The physical properties measurements by Terra Tek showed the bulk density to be 2.723 gm/cm^3, grain density 2.778 gm/cm^3, porosity 1.6%, P-wave velocity 3.742 km/sec, S-wave velocity 2.384 km/sec, and Poisson's ratio, 0.16. An XRD analysis [Martin, 1993] revealed a mineralogy of 37% quartz, 12% plagioclase, 12% calcite, 7% ferroan dolomite, 3% pyrite, 8% chlorite, 16% illite/mica and 5% amorphous (poorly crystalline materials and organic material).

The samples we tested were of comparable density (2.735 - 2.742 gm/cm^3) to the Terra Tek sample. They were homogeneous, massive and competent.

2.2 Experiments conducted

Six impact experiments were conducted at Sandia on this material. The test matrix is summarized in Table 1. All of these experiments were conducted in the reverse-ballistic configuration (sample in projectile). The powder gun and the two-stage light gas gun at the Sandia STAR Facility were used for these tests.

The highest-velocity test was conducted with a tantalum buffer to reach higher pressures. To avoid complications previously encountered with tantalum buffer experiments, associated with a ringing in the aluminum cup, the cup was eliminated and the sample impacted the tantalum directly. The main disadvantage of this configuration is that the sample is subjected to gun vacuum, and possible consequent desiccation. (An alternative, using a tantalum cup as well as a tantalum buffer, was discarded because tantalum melting would occur at the extremely high impact velocities of this experiment.) Prior to performing this test, a scrap of slate was subjected to vacuum in a bell jar for approximately 30 minutes. The loss of density was negligible (about 0.0008%), and could be attributed to loss of adsorbed surface moisture as easily as to bulk water content decrease.

Table 2.1. Test matrix for impact studies of Pennsylvania Slate, with schematics

Shot #	Gun Facility	Impact Velocity (km/sec)	Foam Density (gm/cm^3)	Foam Thick (mm)	Sample ID	Sample Density (gm/cm^3)	Sample Thick (mm)	Al Cup Thick (mm)	Buffer Material[1]	Buffer Thick (mm)	Window[2] Thick (mm)	Velocity[3] Per Fringe (km/sec)
SLP1	Powder	0.715	0.291	5.006	Slate#1	2.7405	6.025	2.523	Al	1.487	25.444	0.1565
SLP2	Powder	1.161	0.297	4.978	Slate	2.742	5.997	1.721	Al	1.488	25.446	0.1983
SLP3	Powder	1.951	0.619	5.077	Slate	2.741	6.026	2.005	Al	1.485	25.332	0.2717
SLP4	2-Stage	3.04	0.779	2.249	Slate#5	2.735	4.018	0.980	Al	0.970	19.205	0.4276
SLP6	2-Stage	6.44	0.780	2.258	Slate#6	2.737	4.017	No Cup	Ta	3.096	19.226	1.0192
SLP7	2-Stage	5.83	0.777	2.256	Slate	2.734	4.014	1.017	Al	1.017	19.203	0.6726

[1]Standard aluminum used is 6061-T6 throughout assembly.

[2]Window is composed of lithium fluoride for reverse-ballistic tests in this study.

[3]Velocity per fringe (VPF) corresponds to a setting of the VISAR. Assuming $\Delta v/v=0.28$

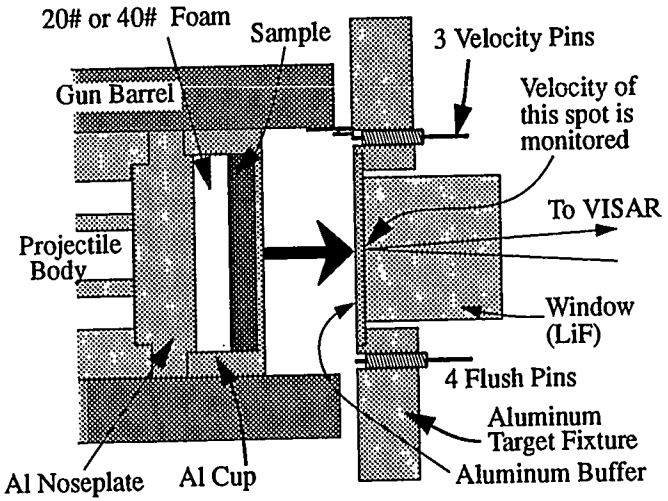

Powder gun experiments (SLP 1, 2, 3)

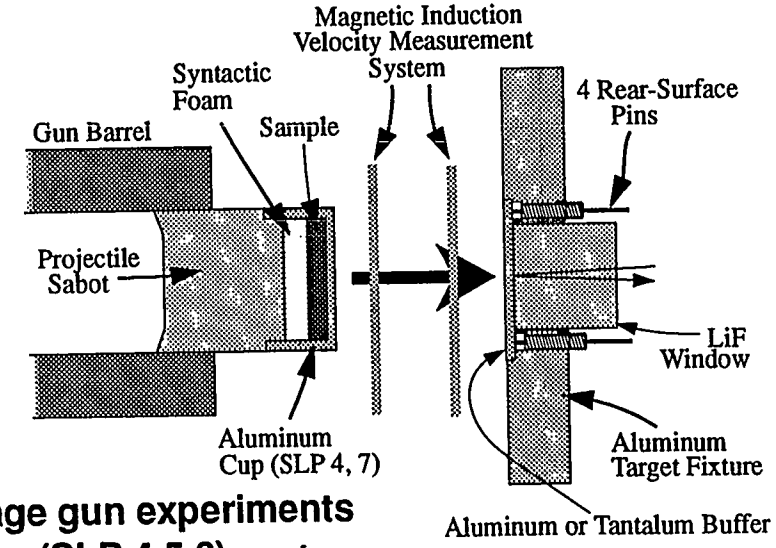

2-stage gun experiments (SLP 4,5,6)

2.3 Dynamic properties results

2.3.1 Observed velocity profiles

Figures 2-1 and 2-2 show the wave profiles observed for these tests. Tests SLP 1 - 4 and SLP 7 show relatively clean profiles, similar to the idealized profile in Figure 1-2. A signature of a gap between the sample and the cup is present for tests SLP 1, 2, 4, and 7. Calculated gap widths are summarized in Figures 2-1 and 2-2. Late-time velocities (~4 μs after impact) vary from 5% to 20% of the plateau velocity (~2 μs after impact) with the density of foam chosen to back the sample. The profile from SLP 6 (Ta buffer) is somewhat noisier than the others, but the noise level is of sufficiently small amplitude and high frequency that it did not reduce the usability of the data. Note that the form of this profile is different from that of the others because there is no cup; the deceleration at 1.0 - 1.3 μsec after impact is a signature of the release propagated through the sample from the sample-foam interface (modified by a spall in the tantalum).

Timing relative to impact is established through use of the shock properties of the buffer materials, using values in Table 2.2.

Table 2.2 Ancillary material equation-of-state parameters assumed*

Material	ρ_0 (kg/m^3)	C_0 (m/sec)	S	γ_0	Y (GPa)
Lithium Fluoride	2641	5148	1.35	1.63	0.2
Aluminum	2698	5370	1.34	2.1	0.3
Tantalum	16680	3293	1.31	1.6	0.7

*Assuming linear shock velocity/particle velocity relation ($U_s = C_0 + SU_p$). Y = dynamic yield strength

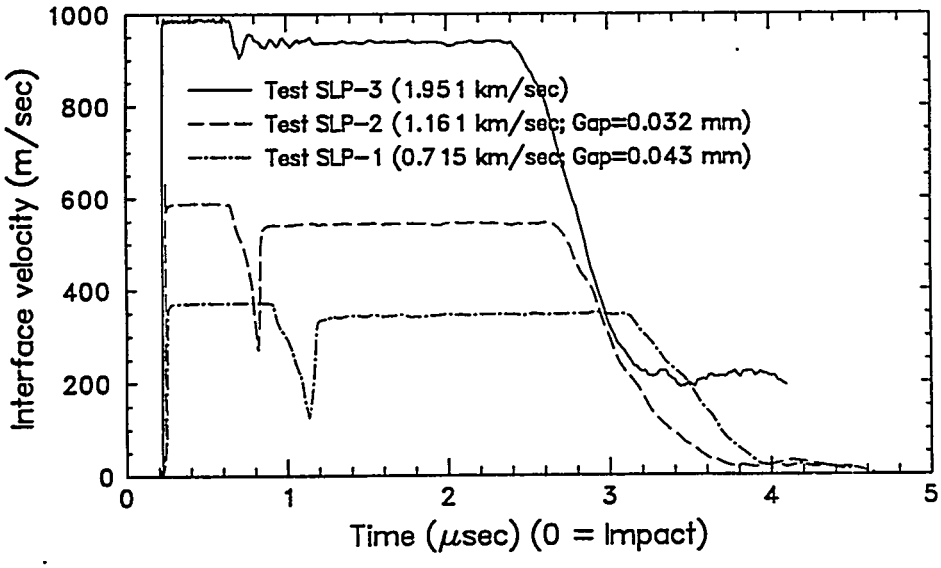

Figure 2-1. Velocity profiles for powder gun tests on Pennsylvania Slate.

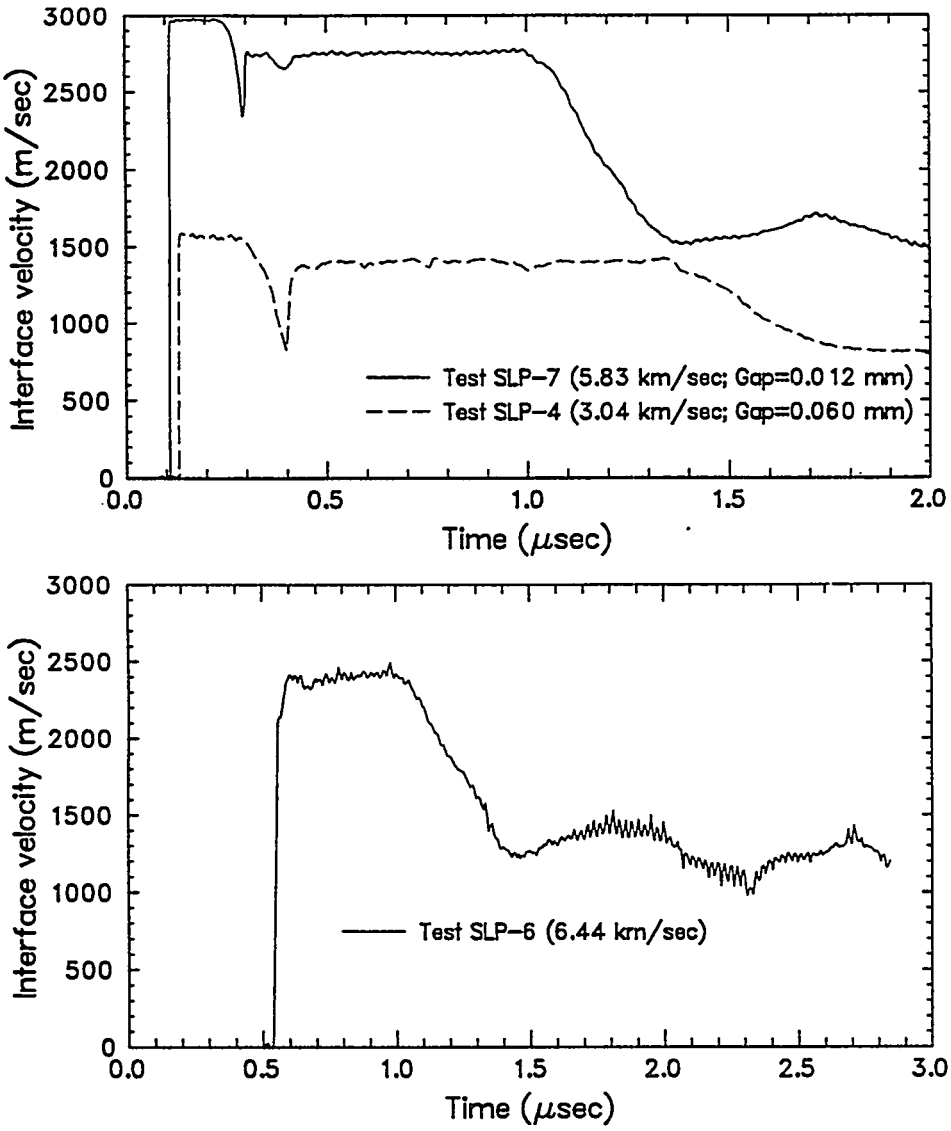

Figure 2-2. Velocity profiles for 2-stage gun tests on Pennsylvania Slate

2.3.2 Hugoniot and release properties

Hugoniot conditions were calculated by standard impedance-match methods [Furnish, 1993a, b]. The input data for these calculations are the projectile velocity, the sample density and the observed plateau velocity on the measured velocity profiles (the level of the long plateaus in Figures 2-1 and 2-2). As well, information is needed about the shock properties of the cup, the buffer and the window.

Table 2.3 summarizes the Hugoniot conditions calculated from these tests, together with uncertainties due to errors in projectile velocity measurement, measurement of the plateau level on the waveforms, initial density error, and errors in the ancillary material equations-of-state. Projectile velocity errors are the most important contributions to errors in the calculated quantities, although uncertainties in the ancillary material EOS contributed significantly as well.

Table 2.3. Hugoniot conditions for Pennsylvania Slate experiments

Shot #	Proj. Velocity km/sec	Observed Vel. km/sec	ρ_0 gm/cm^3	Hugoniot Conditions: Particle Vel km/sec	Pressure GPa	ρ gm/cm^3	Shock Vel. km/sec	ρ/ρ_0	Specific Vol cm^3/gm
1	0.715(8)	0.345(3)	2.741(2)	0.376(9)	5.2(1)	2.96(1)	5.08(17)	1.080(5)	0.338(1)
2	1.161(14)	0.543(2)	2.742(2)	0.628(15)	8.6(1)	3.13(2)	5.00(14)	1.143(8)	0.319(2)
3	1.95(2)	0.939(3)	2.741(2)	1.03(2)	16.3(3)	3.34(3)	5.77(16)	1.217(13)	0.300(3)
4	3.04(4)	1.398(10)	2.735(2)	1.67(4)	26.6(5)	3.83(9)	5.83(18)	1.40(3)	0.261(6)
7	5.83(2)	2.750(7)	2.734(2)	3.12(4)	65.7(9)	4.60(8)	7.70(14)	1.68(3)	0.217(4)
6	6.44(6)	2.40(2)	2.737(2)	4.87(7)	139.7(2.5)	5.12(16)	10.48(26)	1.87(5)	0.195(6)

(Note that values in parenthesis represent uncertainties in the last 1-2 digits of the quantity. Experiment 6 was conducted with a tantalum buffer.)

Release paths have been calculated from the waveforms, and are plotted together with the Hugoniot points and associated uncertainties, in Figures 2-3 through 2-5. The procedure for this calculation is presented in Appendix B. Model waveforms corresponding to these release paths are shown in Appendix B (Figures B-1 and B-2). Release paths are tabulated in Appendix A.

As mentioned above, related data were obtained at the DNA Impact Facility by Ktech Corp. [Davies and Smith, 1994]. Nine tests, including 5 with carbon gauges and 4 with VISAR, yielded wave profile and Hugoniot data over the stress range 0.4 - 10 GPa. These are plotted against the present results (the 4 lowest-pressure tests) in Figures 2-3 through 2-5.

Test SLP-2 of the present series appears to have an anomalously low shock velocity; otherwise the two sets of data are in good agreement. A similar dip, over the particle velocity range 0.3 - 0.8 km/sec (stress range 3 - 8 GPa) was observed by Anderson et. al. [1995] in a suite of measurements on Yellow Shale obtained from Marble Mtn., CA. If a two wave loading structure occurs under the conditions of test SLP-2, our data reduction method would lead to an erroneous calculation of the Hugoniot shock velocity and sample density. However, there is no evidence for such a structure in the Ktech wave profiles acquired for a forward-ballistic geometry (sample in target) [Davies and Smith, 1994]. Hence there is no obvious reason to suppose that the calculated Hugoniot state for test SLP2 is in error.

The releases appear to be slightly hysteretic (i.e. below Hugoniot) for pressures less than 30 GPa, and normal (i.e. above Hugoniot) for pressures greater than 60 GPa, consistent with the behavior observed for tuffs and granites [Furnish, 1993b]. Typically this change from hysteretic to normal release behavior occurs at between 40 and 60 GPa in rocks.

Several sensitivity studies were undertaken. As a measure of the hysteresis of the release, the two lowest-pressure tests were modeled using an assumed Mie-Grüneisen release behavior (no strength). The resulting model waveforms and stress-density release paths

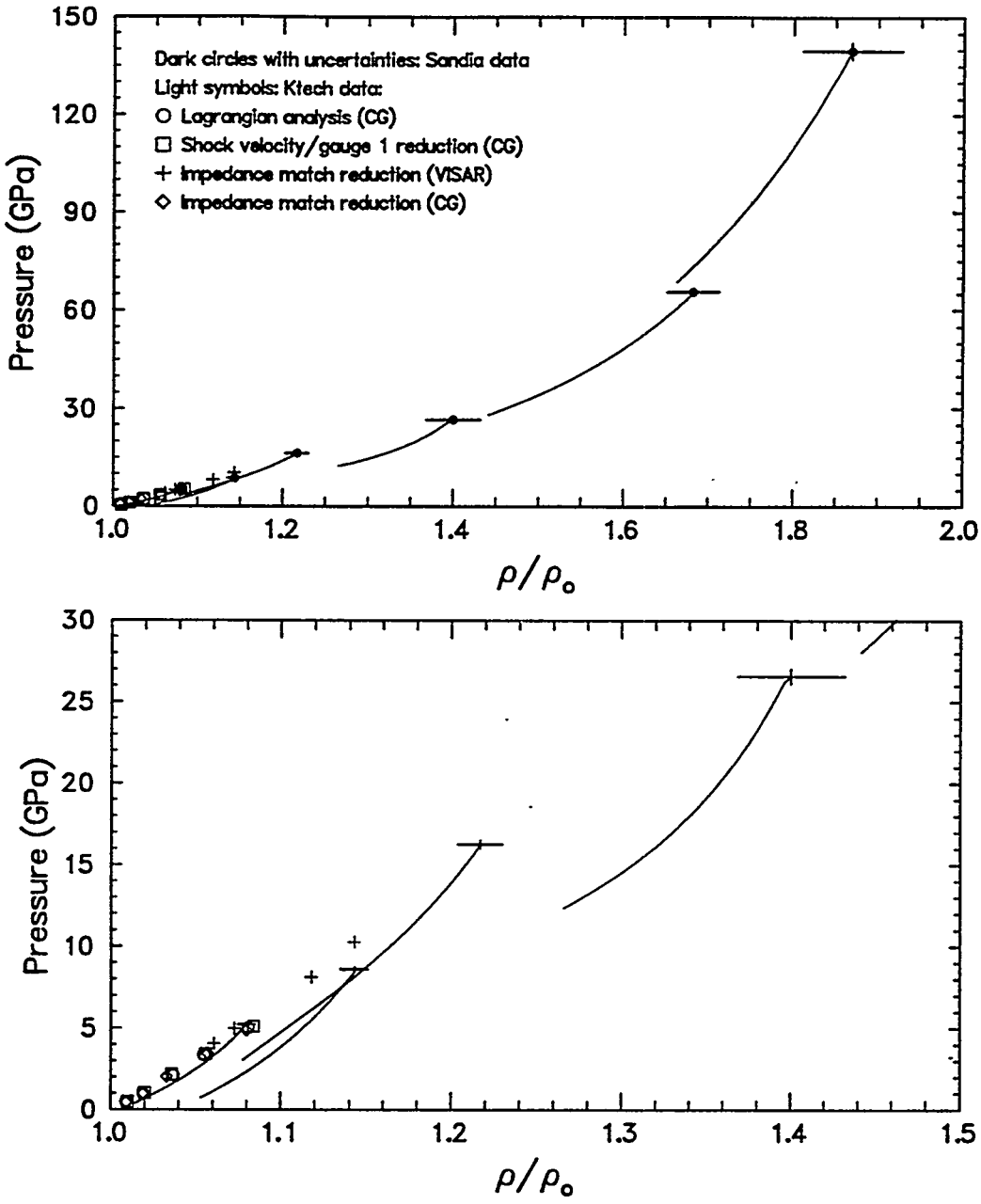

Figure 2-3. Hugoniot and release results for Pennsylvania Slate (P vs. ρ/ρ_0)
(Top) Entire range of experiments; (Bottom) Detail of lower portion of range.

are shown in Figure 2-6. The Mie-Grüneisen release behavior assumption gives a much poorer match to the observed wave profiles than does the modulus fit. Note that a smaller slope in the release (lower $\delta P/\delta\rho$) gives a later release arrival.

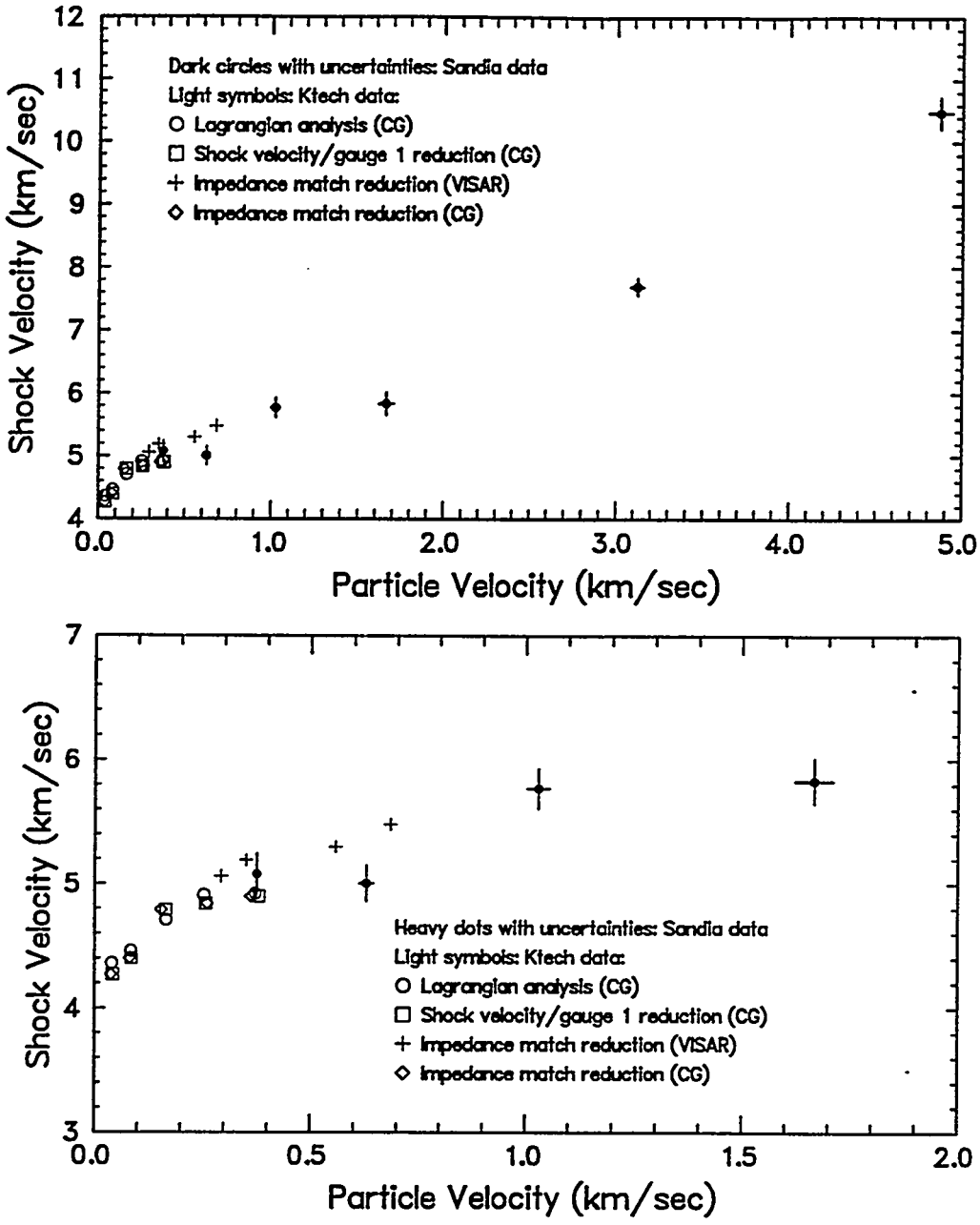

Figure 2-4. Hugoniot and release results for Pennsylvania Slate (U_S/U_P space). (Top) Entire range of experiments; (Bottom) Detail of lower portion of range.

For the tantalum-buffer experiment, four parameters were perturbed: (1) The tantalum strength was changed to 4 kb from 7 kb; (2) An alternative fit to the tantalum Hugoniot was used ($C_0 = 3.414$ km/sec, $S = 1.201$, $\rho_0 = 16.650$ gm/cm^3, vs. $C_0 = 3.293$ km/sec, $S = 1.307$, $\rho_0 = 16.680$ gm/cm^3); (3) The tantalum spall strength was changed to 4 GPa from 6

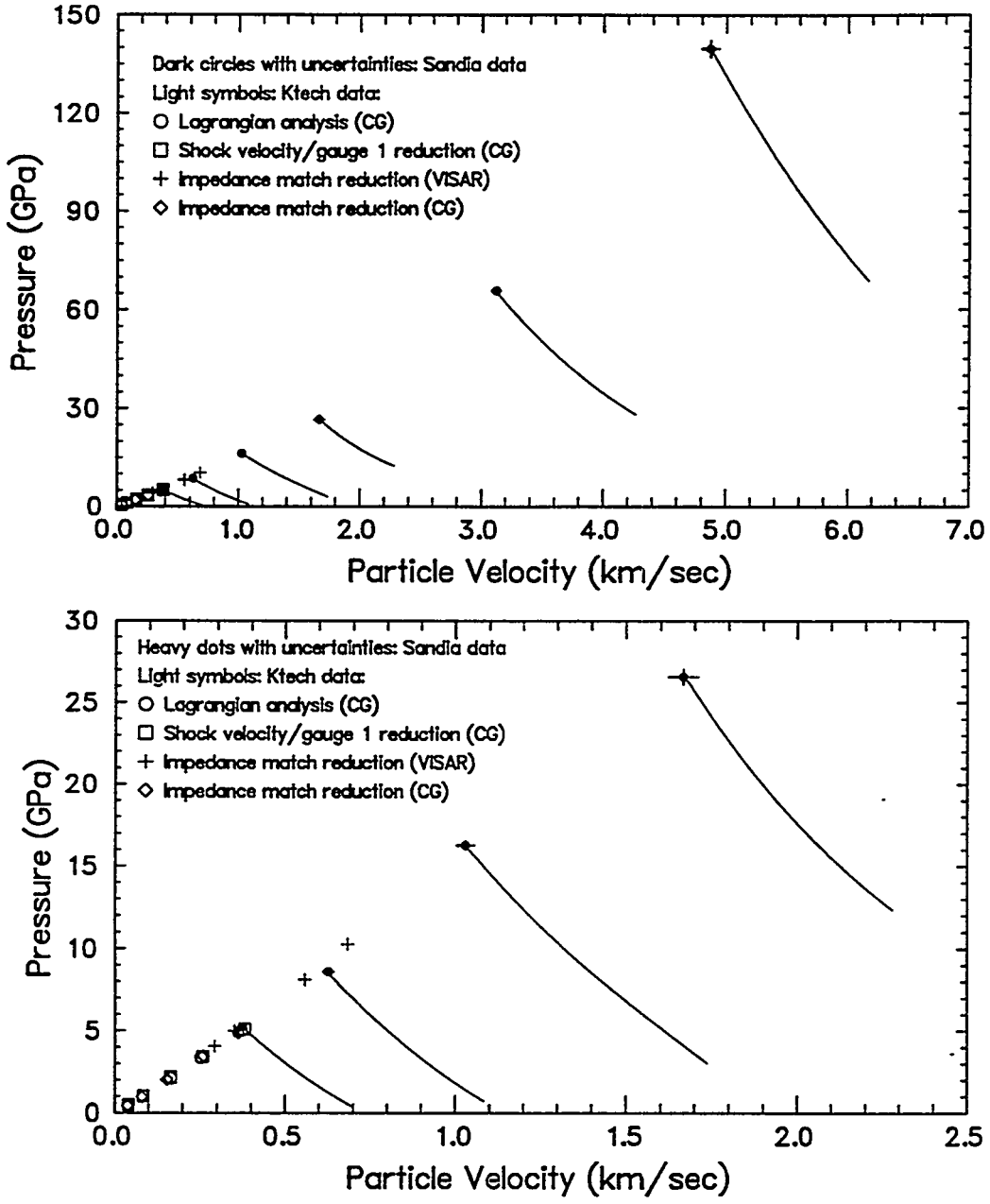

Figure 2-5. Hugoniot and release results for Pennsylvania Slate (P vs. U_P space) (Top) Entire range of experiments; (Bottom) Detail of lower portion of range.

GPa; and (4) B_0 was changed from 1700 GPa to 2000 GPa. The results are shown in Figure 2-7. Reassuringly, the only variation of the tantalum EOS which significantly affected the calculated velocity profile in the interval of interest was the deliberate change in the release modulus used (B_0 adjustment).

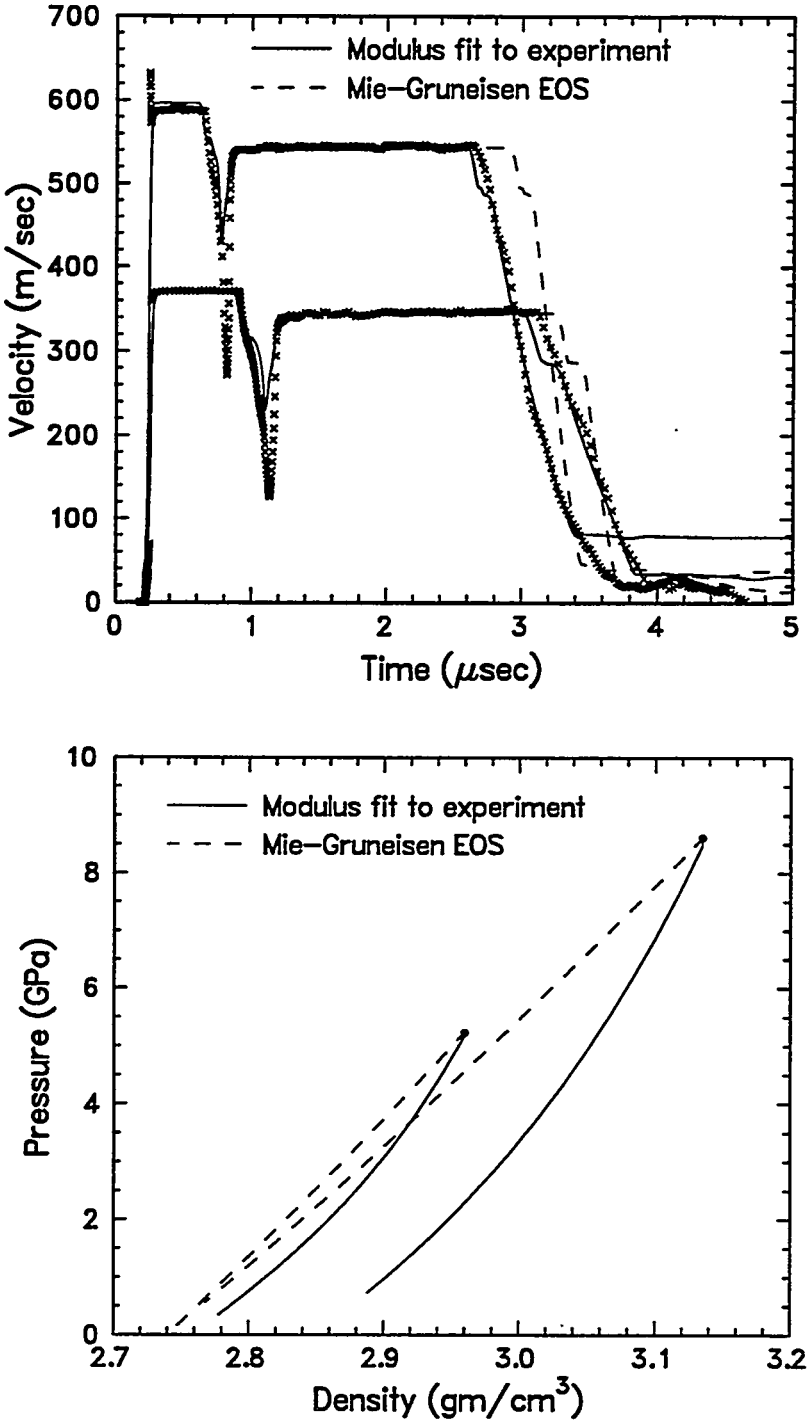

Figure 2-6. Waveforms and P - ρ release paths calculated for (1) Mie-Grüneisen EOS on compression and release, and (2) modulus fit to experimental waveform. Tests SLP1, 2

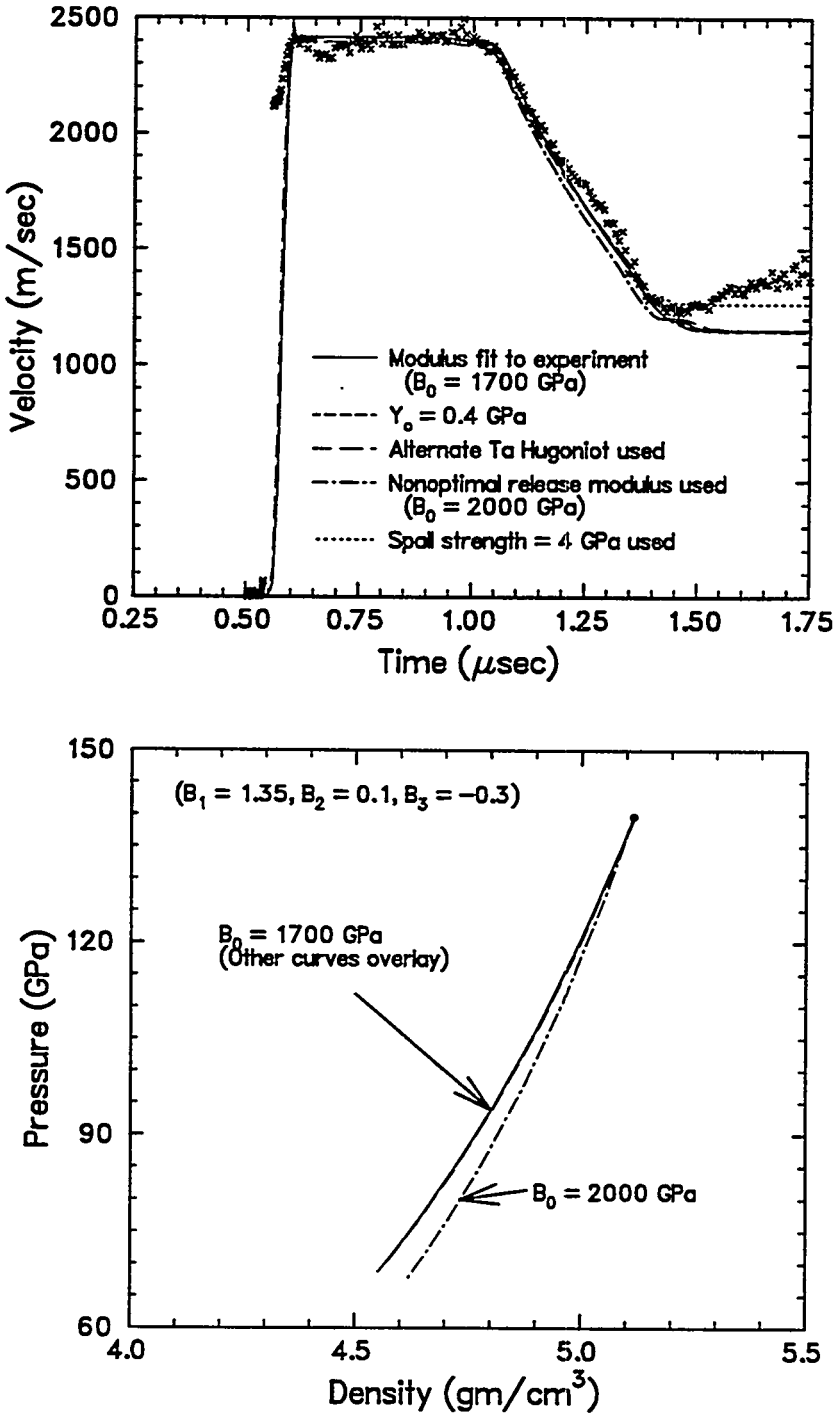

Figure 2-7. Waveforms and pressure - density release paths calculated for various trial adjustments of tantalum EOS for test SLP 6.

3.0 Impact Tests on Phyllite

3.1 Materials studied

As a portion of the HYDROPLUS project, DNA undertook to assess whether the equation-of-state of a relatively low-porosity rock which is frozen *in-situ* is changed significantly by thawing or by thawing and refreezing. Several rock materials were recovered from the Lupin mine in Canada, including samples of phyllite and of quartzite. These materials underwent extensive mechanical and compositional characterization testing (see Martin *et al* [1992]). Sandia performed a suite of impact tests on the quartzite over the 1 - 9 GPa stress range, combining forward and reverse-ballistic testing under various temperature conditions [Furnish, 1993a]. Ktech Corp. performed a suite of tests on the phyllite over the stress range 0.8 - 8 GPa [Davies and Smith, 1994]. In general, the conclusion was reached that for these very-low-porosity materials, the frozen/thawed state does not affect material behavior in a way that needs to be accounted for in the attenuation calculations.

In the present section, we document three additional, higher-stress tests on the phyllite. All of these tests were conducted at room temperature. The samples were from the same batch of cores as were the samples tested by Davies and Smith [1994]. The core designator (as provided by Terra Tek [Martin, 1993a]) is Lu#2, 5.36-5.45'. The samples were prepared to Sandia specifications by Terra Tek. No attempts were made to preserve water saturation or to desiccate the samples because of their low porosity.

The phyllite is from the (Archean) Contwoyto Formation. The lithologic description is as follows [Martin *et al*, 1992, pp. 13]:

> Grayish-black to black with greenish black tint; very hard, dense; trace biotite; trace disseminated pyrite; foliation cuts core at 40 to 70° angle. Rare 1 to 4 mm wide calcite-filled fractures, usually with disseminated or intermittent pyrite fractures, typically tight with no visible porosity, and vary from single planar fractures parallel to foliation to branching and intersecting patterns crossing foliation. Several calcite and pyrite coated core partings show slickenside lineations. A calcite filled fracture in LU #2A, run #6, 1 cm wide with vuggy porosity along center of vein; calcite crystals up to 8 mm across; water ice fills void.

Although a compositional analysis is not available immediately adjacent to the core tested, sample Lu#2 at the 9.11 m level was found to be 13 wt% quartz, 19 wt% plagioclase, ~2 wt% feldspar, 5 wt% calcite, 37 wt% muscovite and 24 wt% chlorite [Martin *et al*, 1992].

3.2 Experiments conducted

The test matrix is summarized in Table 3.1. Reverse-ballistic geometries were used throughout. Impact conditions were chosen to provide nominal Hugoniot stress levels of

Table 3.1. Test matrix for impact studies of phyllite, with schematics

Shot #	Gun Facility	Impact Velocity (km/sec)	Foam Density (gm/cm^3)	Foam Thick (mm)	Sample ID	Sample Density (gm/cm^3)	Sample Thick (mm)	Al Cup Thick (mm)	Buffer Material[1]	Buffer Thick (mm)	Window[2] Thick (mm)	Velocity[3] Per Fringe (km/sec)
Phy1	Powder	1.69	0.620	5.047	Phyllite	2.760	6.042	n.a.	Al	1.440	25.324	0.35308
Phy2	2-Stage	3.735	0.779	2.242	Phyllite	2.770	4.027	n.a.	Al	0.773	19.169	0.68512
Phy3	2-Stage	4.89	0.779	2.297	Phyllite	2.772	4.014	0.895[4]	Al	0.973	19.184	0.76886

Notes:

[1]Standard aluminum used is 6061-T6 throughout assembly.

[2]Window is composed of lithium fluoride for all tests in this study.

[3]Velocity per fringe (VPF) corresponds to a setting of the VISAR. Assuming $\Delta v/v_0=0.28$

[4]Cup used for this test because of concern for condition of sample

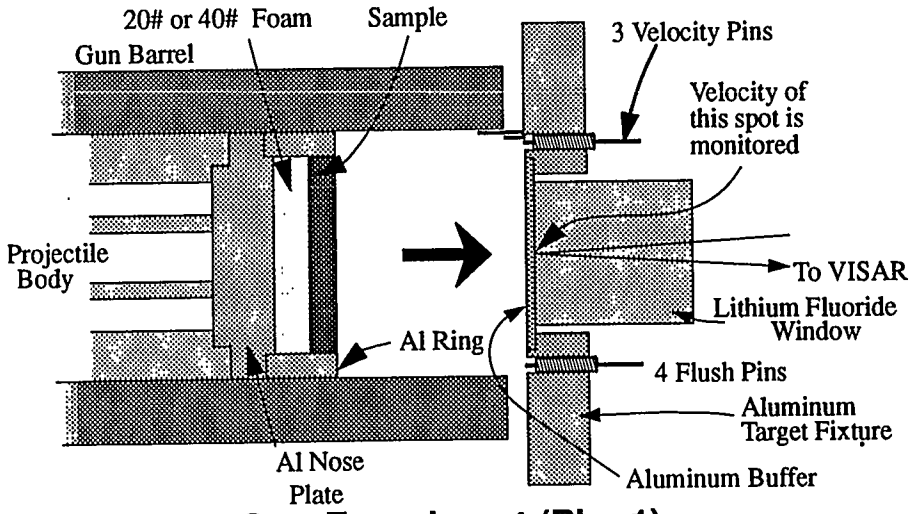

Powder Gun Experiment (Phy 1)

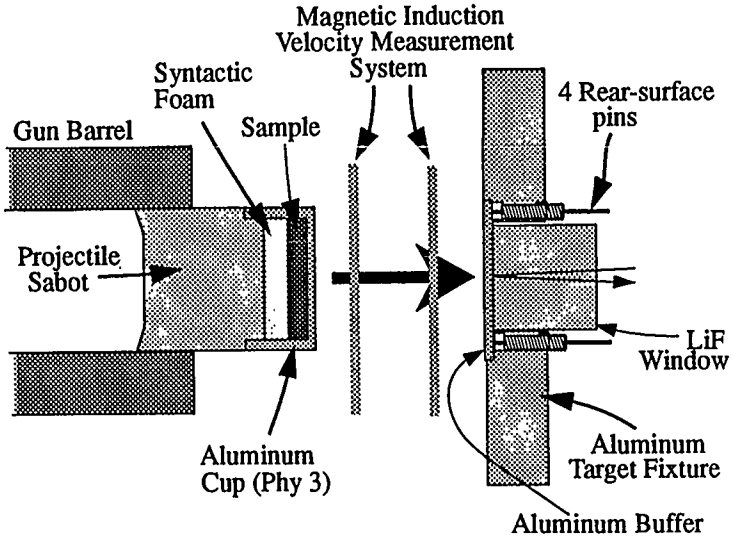

2-Stage Gun Experiments (Phy 2, 3)

150, 350 and 500 kb; this required the use of the powder gun (1 test) and the 2-stage light gas gun (2 tests). The two lower-stress experiments were conducted with uncontained samples, while the highest-stress experiment utilized an aluminum cup (as shown in Figure 1), primarily to insure sample survival during the launch. Sample survival was a concern because the sample used in test Phy 3 had a slight crack near one edge (11.34 mm from center).

Our measured densities averaged 2.77 gm/cm^3, which is about 1% below the densities quoted for the samples tested by Ktech. The samples were homogeneous, massive and competent.

3.3 Dynamic properties results

3.3.1 Observed velocity profiles

Figure 3-1 shows the velocity profiles observed for these tests. Timing relative to impact was accomplished by calculating shock transit time through the aluminum buffers and

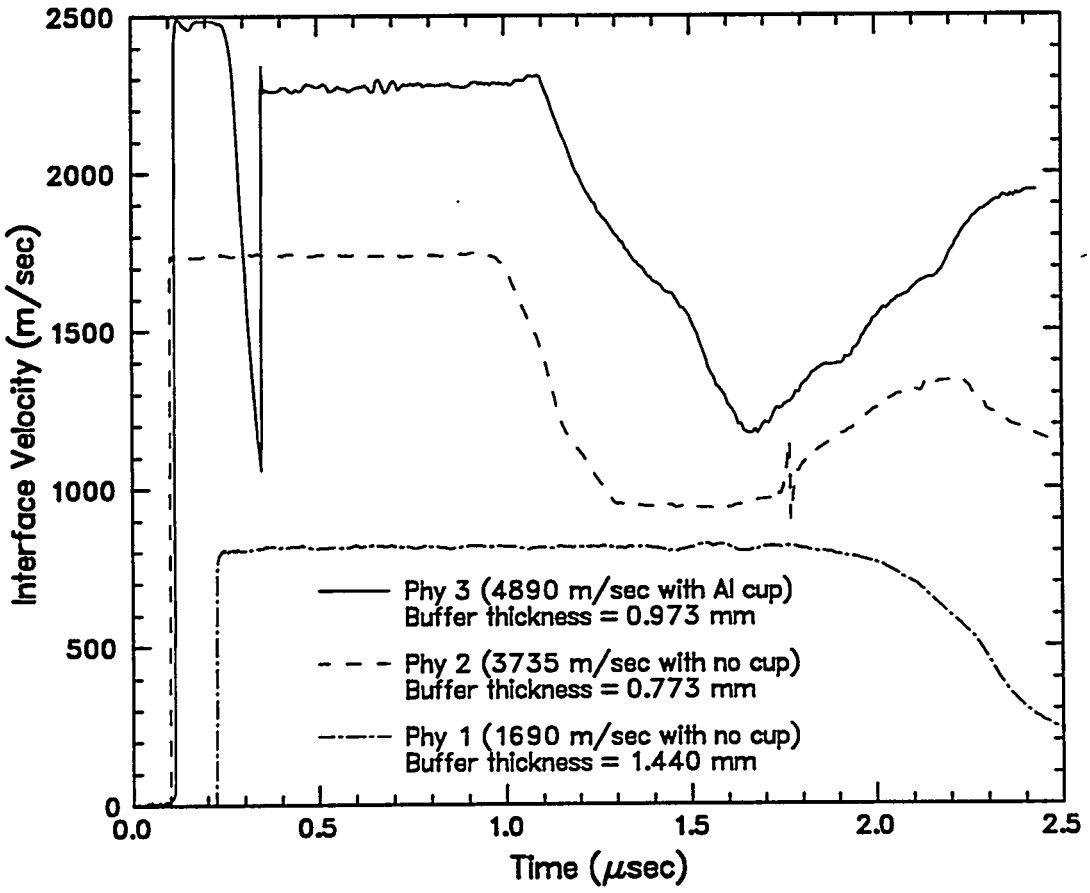

Figure 3-1. Velocity profiles for phyllite tests.

shifting the traces accordingly. This is an accurate (~5 nsec) method which requires far less effort than fiducial-based timing.

The most obvious variation between profiles, the higher initial plateau in test Phy 3 which is lacking in the lower-velocity experiments, is due to the use of a cup in Phy 3. A gap signature is also visible in the profile for Phy 3, indicating that a very slight gap (not more than 100 μm) developed between the sample and the cup. Another variation is seen in the corner structure at the start of the release (becoming sharper for the upper stress levels), which may be an artifact of wave processing in the aluminum.

3.3.2 Hugoniot and release properties

The Hugoniot conditions were calculated using standard impedance-match methods [Furnish, 1993a,b]. Results are summarized in Table 3.2 and Figures 3-2 and 3-3, together with

Table 3.2. Hugoniot conditions for phyllite experiments

				Hugoniot Conditions					
Shot #	Proj. Velocity km/sec	Observed Vel. km/sec	ρ_0 gm/cm^3	Particle Vel km/sec	Pressure GPa	ρ gm/cm^3	Shock Vel. km/sec	ρ/ρ_0	Specific Vol cm^3/gm
1	1.69(1)	0.814(3)	2.760	0.891(11)	13.73(8)	3.28(2)	5.59(9)	1.189(6)	0.304(1)
2	3.73(2)	1.738(4)	2.770	2.03(3)	35.19(12)	4.09(4)	6.27(7)	1.478(14)	0.244(2)
3	4.89(2)	2.273(13)	2.772	2.65(2)	50.4(4)	4.52(7)	6.85(10)	1.632(24)	0.221(3)

(Values in parenthesis represent uncertainties in the last 1-2 digits of the quantity)

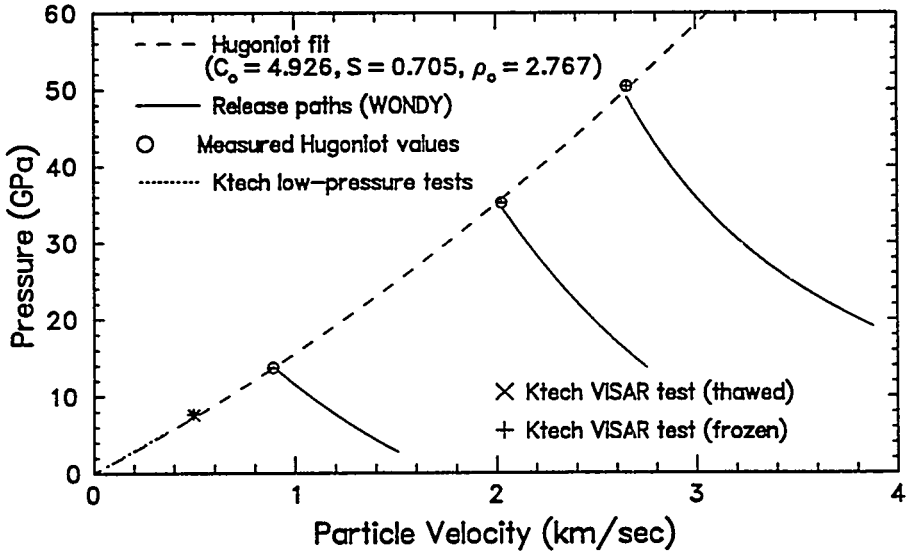

Figure 3-2. P - U_P representation of Hugoniot and release paths for phyllite tests. "Ktech" data are from Davies and Smith [1994].

uncertainties due to errors in projectile velocity measurement, measurement of the plateau level on the waveforms, initial density error, and errors in the ancillary material equations-of-state. A fit Hugoniot is included for interpretation. The release paths are derived in the usual way (see Appendix B), through wavecode matches using an adjustable Lagrangian release modulus. The wavecode fits to the velocity profiles are shown in Appendix B (Figure B-3).

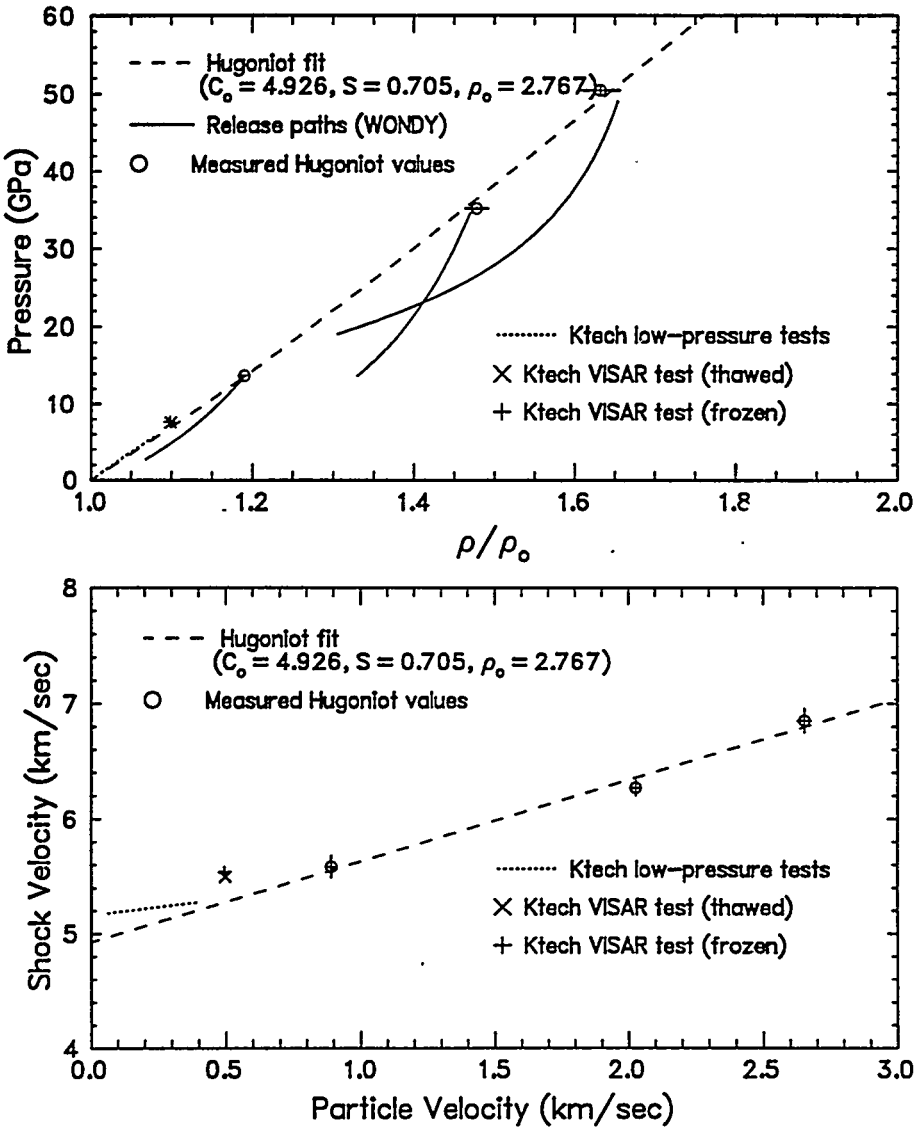

Figure 3-3. P - ρ/ρ_0 and U_S - U_P representations of Hugoniot and release results for phyllite tests. "Ktech" data are from Davies and Smith [1994]

For comparison, the results of Davies and Smith [1994] are plotted against the present data in Figures 3-2 and 3-3, labeled as "Ktech." The lower-pressure data (13 forward-ballistic tests utilizing carbon gauges) from their set are well represented by the short dotted segment, while the upper two Hugoniot points (forward-ballistic with VISAR diagnostics) deviate somewhat from it. These data appear to be consistent with the present set, with no evidence of significant phase transitions between the stress regimes spanned by the individual data sets.

It is interesting how strongly hysteretic the two highest-pressure releases are. This may be the effect of hysteresis in the $^{IV}SI \leftrightarrow {}^{VI}Si$ phase transition observed for quartz and other silicates (known as "quartz $\leftrightarrow$ stishovite" for pure silica).

4.0 Impact Tests on Granite

4.1 Materials studied

A granite from the SHIST site (White Sands, NM) was supplied for testing. These samples were taken from Core Hole #2, depth interval 118.84 - 119.00 feet. Densities ranged from 2.552 to 2.568 gm/cm^3 (SNL measurements) or 2.564 to 2.574 gm/cm^3 [Marquartd, 1993].

The mineralogy of an adjacent (Hole #2, 104.9') granite was described by Martin [1993b] as 32% (wt.) quartz, 22% plagioclase, 34% potassium feldspar, 2% calcite, 4% chlorite and 6% illite/mica (last is probably dominantly biotite). Physical properties of samples from two close samplings are presented in Table 4.1.

Table 4.1. Physical properties of SHIST test plugs*

Sample ID	Hole #2 115.5'	Hole #2 124.1'
Bulk Density (gm/cm^3)	2.596	2.603
Effective Grain Density (gm/cm^3)	2.616	2.613
Effective Porosity (%)	0.75	0.35
True Grain Density (gm/cm^3)	2.636	2.635
Total Porosity (%)	1.45	1.25
Occluded Porosity (%)	0.7	0.9

*Properties are averaged values for samples acquired parallel and perpendicular to the hole at approximately the specified depth. Data from Martin [1993b].

4.2 Experiments conducted

Four tests were conducted, designed to sample the stress range of 10 - 20 GPa. Three were conducted in the reverse-ballistic mode. The fourth was conducted in the forward-ballistic (transmitted-wave) mode to obtain loading data. The detailed test matrix is presented in Table 4.2.

4.3 Dynamic properties results

4.3.1 Observed velocity profiles

Observed velocity profiles are shown in Figure 4-1. Timing in the reverse-ballistic tests was established using the predicted shock transit time through the aluminum buffer. Impact time for the forward-ballistic test (GR 4) was established by comparing fiducial timing with that for the reverse-ballistic tests (error estimated as < 35 nsec). Since no

Table 4.2. Test matrix for impact studies of granite, with schematics

Shot #	Gun Facility	Impact Velocity (km/sec)	Foam Density (gm/cm^3)	Foam Thick (mm)	Sample ID	Sample Density (gm/cm^3)	Sample Thick (mm)	Al Cup/ Impactor Thk (mm)	Buffer Material[1]	Buffer Thick (mm)	Window[2] Thick (mm)	Velocity[3] Per Fringe (km/sec)
GR 1	Powder	1.392	~0.32	~8	Granite#1	2.568	4.984	n.a.	Al	1.393	25.417	0.27048
GR 2	Powder	2.168	~0.64	~5	Granite#2	2.559	4.992	n.a.	Al	1.418	25.382	0.35308
GR 3	Powder	2.331	~0.64	~5	Granite#3	2.552	4.979	n.a.	Al	1.408	25.338	0.43107
GR 4	Powder	1.353	~0.32	~8	Granite#4	2.557	4.983	5.013	n.a.	n.a.	25.412	1.04837

Note that Gr 4 is a forward-ballistic experiment

[1]Standard aluminum used is 6061-T6 throughout assembly.

[2]Window is composed of lithium fluoride for all tests in this study.

[3]Velocity per fringe (VPF) corresponds to a setting of the VISAR. Assuming $\Delta v/v_0=0.28$

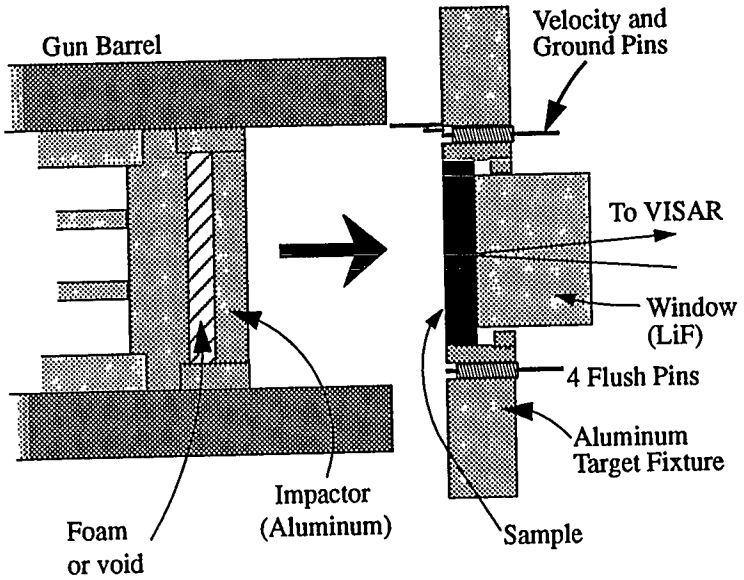

Forward-Ballistics Experiment (GR 4)

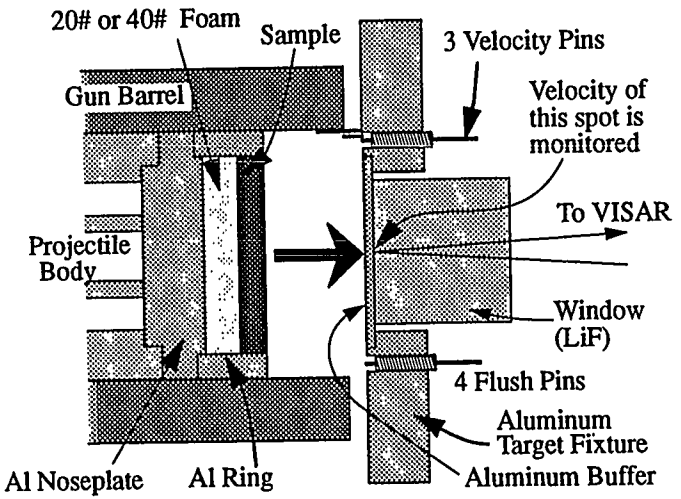

Reverse-Ballistics Experiments (GR 1, 2, 3)

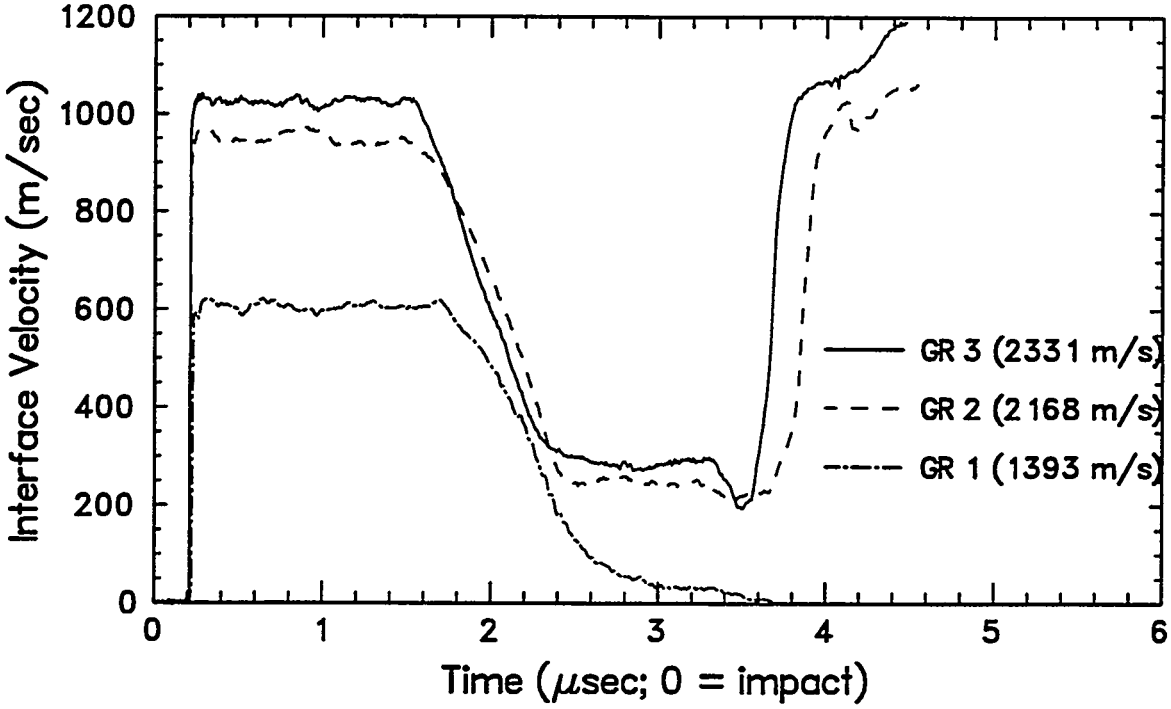

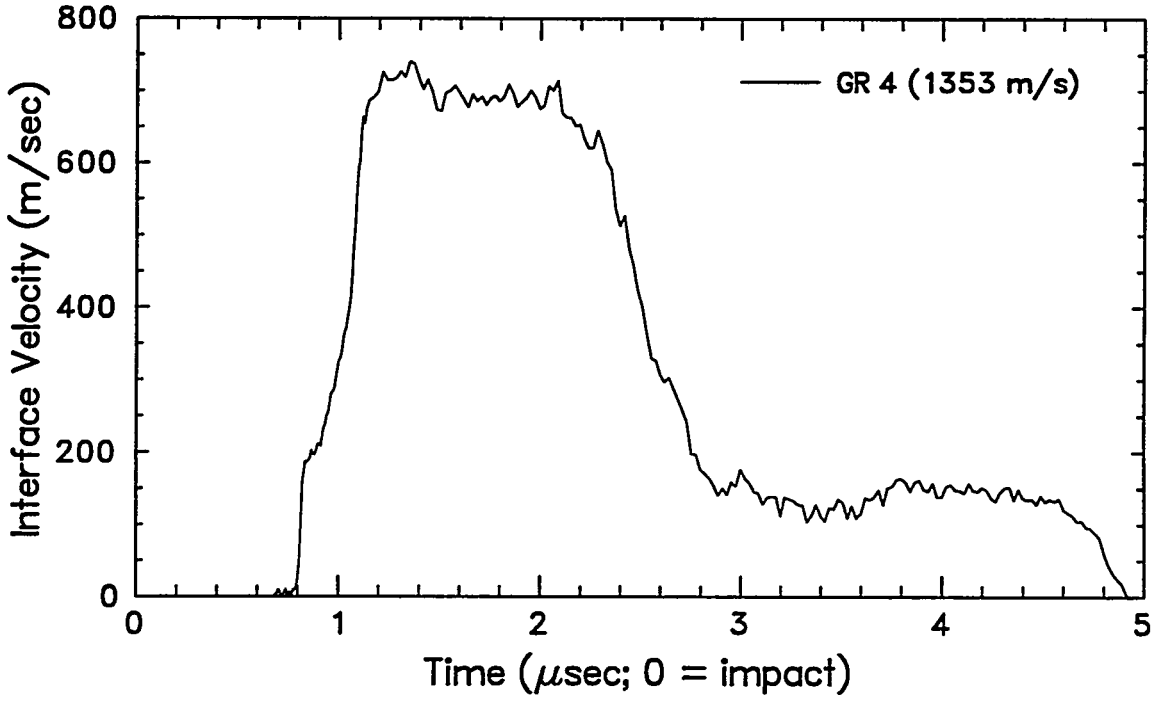

Figure 4.1. Observed velocity profiles for SHIST granite tests.

cups were used to enclose the samples in any of the tests, the reverse-ballistic velocity profiles are simplified (there is no initial plateau). The plateau corresponds to the Hugoniot state of the sample, and the shape and position of the first release reflect the release properties of the sample. A late-time (3.5 - 4 μsec) velocity increase is a reshock caused by the projectile nosetip behind the foam for these samples.

The forward-ballistic waveform (GR 4) shows a classic 2-wave loading structure, composed of an elastic precursor preceding a plastic wave. Although the velocity profile from this test is noisier than those from the reverse-ballistic tests, it is still usable.

4.3.2 Loading, Hugoniot and release properties

The precursor, Hugoniot and reshock points are tabulated in Table 4.3, together with error estimates. They are plotted, together with release paths, in Figures 4-2 and 4-3. The Hugoniot states for the reverse-ballistic tests were calculated by standard impedance-match methods [Furnish, 1993a,b], as with the other tests in this report. In the present case, this calculation assumed a precursor with the conditions calculated for the precursor observed in test GR 4. For the forward-ballistic test (GR 4), the calculation is done by an impedance-match method which requires the projectile velocity, the initial sample density and thickness, the times-of-arrival of the first and second waves, the plateau velocity for the first wave, and the equations-of-state of the impactor and the window. The plateau velocity is not required. Details may be found in Furnish [1993a,b].

Table 4.3. Precursor, Hugoniot and reshock states for SHIST granite tests

Reverse-Ballistic Tests

			Hugoniot Conditions →						
Shot #	Proj. Velocity km/sec	Observed Vel. km/sec	ρ_0 gm/cm^3	Particle Vel km/sec	Pressure GPa	ρ gm/cm^3	Shock Vel. km/sec	ρ/ρ_0	Specific Vol cm^3/gm
GR 1	1.392(14)	0.605(5)	2.568(6)	0.798(16)	9.74(11)	3.10(3)	4.41(37)	1.21(1)	0.323(3)
GR 2	2.168(22)	0.947(10)	2.559(14)	1.239(25)	16.45(22)	3.37(6)	5.06(21)	1.32(2)	0.297(5)
GR 3	2.331(23)	1.025(10)	2.552(16)	1.325(26)	18.10(22)	3.39(6)	5.26(18)	1.33(2)	0.295(5)

Forward-Ballistic Test

				Precursor/Hugoniot Conditions →					
Shot #	Proj. Velocity km/sec	Plastic TOA µsec	ρ_0 gm/cm^3	Particle Vel km/sec	Pressure GPa	ρ gm/cm^3	Shock Vel. km/sec	ρ/ρ_0	Specific Vol cm^3/gm
GR 4	1.353(13)	1.085(35)	2.557(7)						
	Precursor Conditions →			0.182	2.841(4)	2.635(7)	6.114	1.0305	0.3795(10)
	Hugoniot Conditions →			0.776(12)	9.53(17)	3.04(2)	4.46(15)	1.189(9)	0.329(2)

		Partial Reshock Conditions →	
Shot #	Plateau Velocity	Stress	Particle Vel.
GR 4	0.68(2)	11.4(4)	0.68(2)

Note that there is a partial reshock of the sample generated by the impedance mismatch between the sample and the LiF window. The window has a higher shock impedance than does the sample. Impedance-match calculations provide the stress and particle velocity of this reshocked state, but cannot provide the shock velocity of the reshock or the density of the reshocked state. This is because the path from the Hugoniot to the reshock is not known, and a Riemann integration may therefore not be performed from the Hugoniot to the reshock (Furnish, 1993a,b].

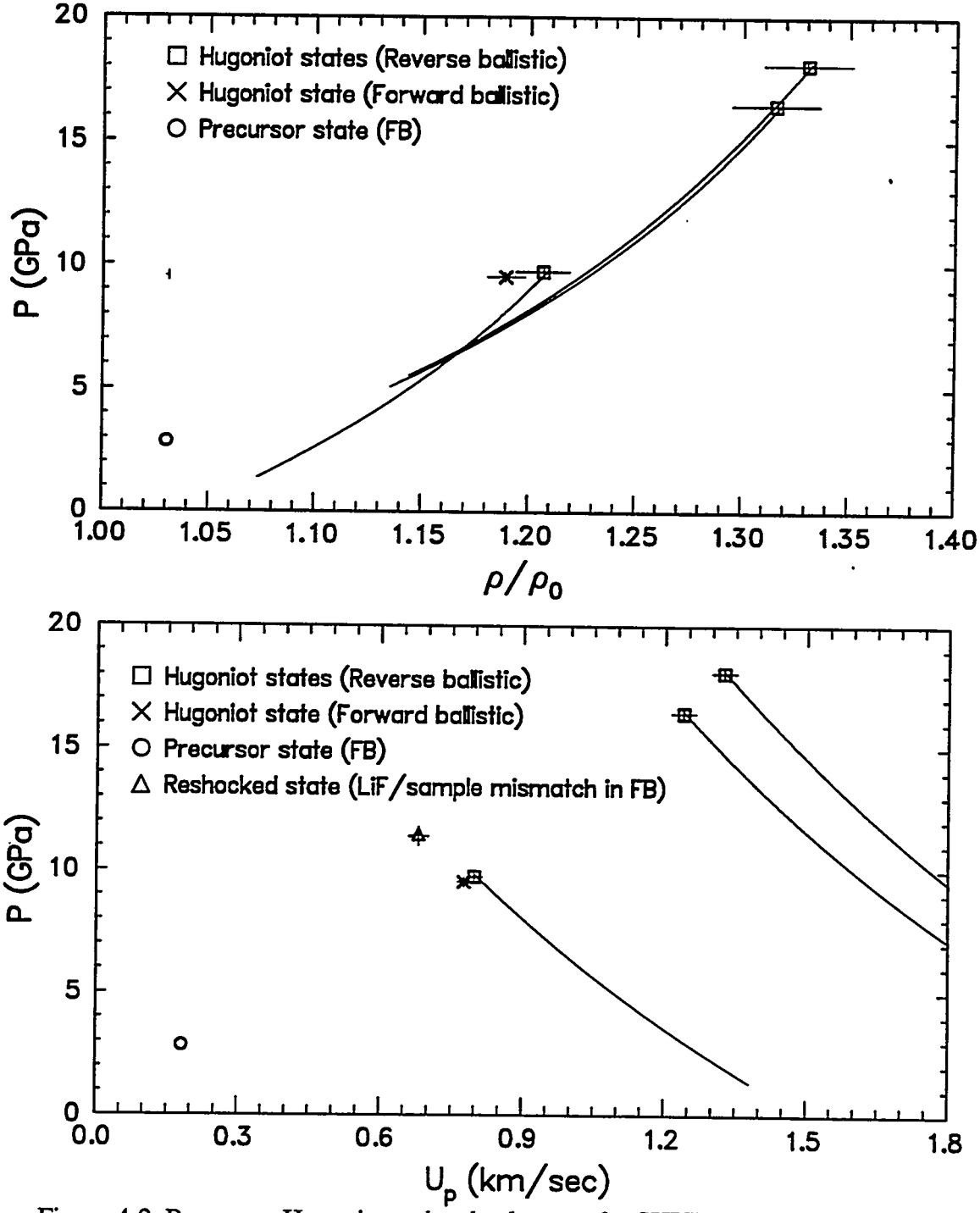

Figure 4-2. Precursor, Hugoniot and reshock states for SHIST granite impact tests.

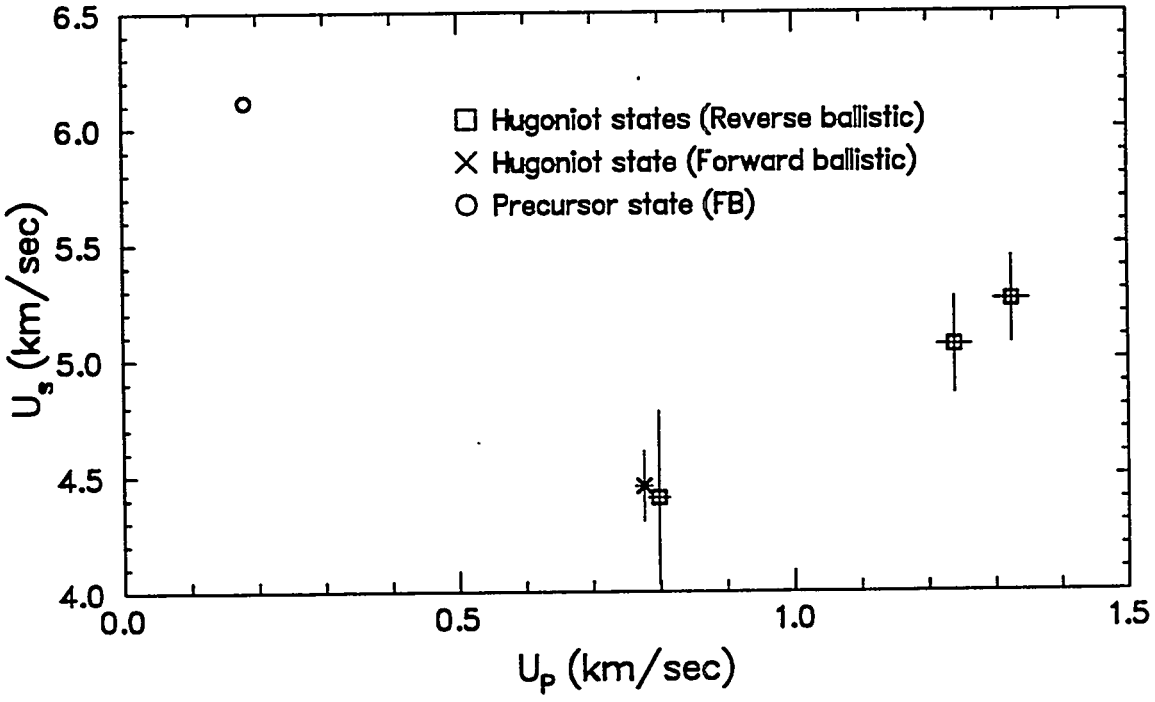

Figure 4-3. Precursor, Hugoniot and reshock states for SHIST granite impact tests.

Release paths for the reverse-ballistic tests were calculated by a procedure described in Appendix B and in Furnish [1993a,b], comprised of modeling the tests with the WONDY V wavecode, and adjusting the parameters governing the release modulus (see Eq. B.1) until the calculated and experimental wave profiles agree. There is one important difference in the modeling of the granite tests: A precursor chosen to match the stress/density conditions observed for test GR 4 (2.841 GPa, 2.646 gm/cm^3) was assumed.

The forward-ballistic test (GR 4) was modeled analogously. The calculated waveforms are plotted against the experimental waveforms in Appendix B (Figure B-4). No attempt was made to model the final reshock in tests GR 2 and GR 3, but most other features of the profiles are modeled.

For the transmitted-wave experiment (GR 4), both WONDY modeling and a Lagrangian wave-evolution analysis were conducted. The wave-evolution approach is based on a comparison between the waveforms observed at the input and the output of the sample; a Lagrangian integration yields a relationship between wave velocity and particle velocity, from which the loading and unloading paths may be calculated in other convenient spaces (see Furnish [1992] for details). The stress-density loops resulting from these two analyses are compared in Figure 4-4, with the impedance-match result for the precursor and Hugoniot state plotted as well. Both analyses are complicated by the reshock (~14% stress jump) caused by the interaction of the loading wave with the sample/LiF interface, and propagating back through the sample. Nevertheless, they agree reasonably well.

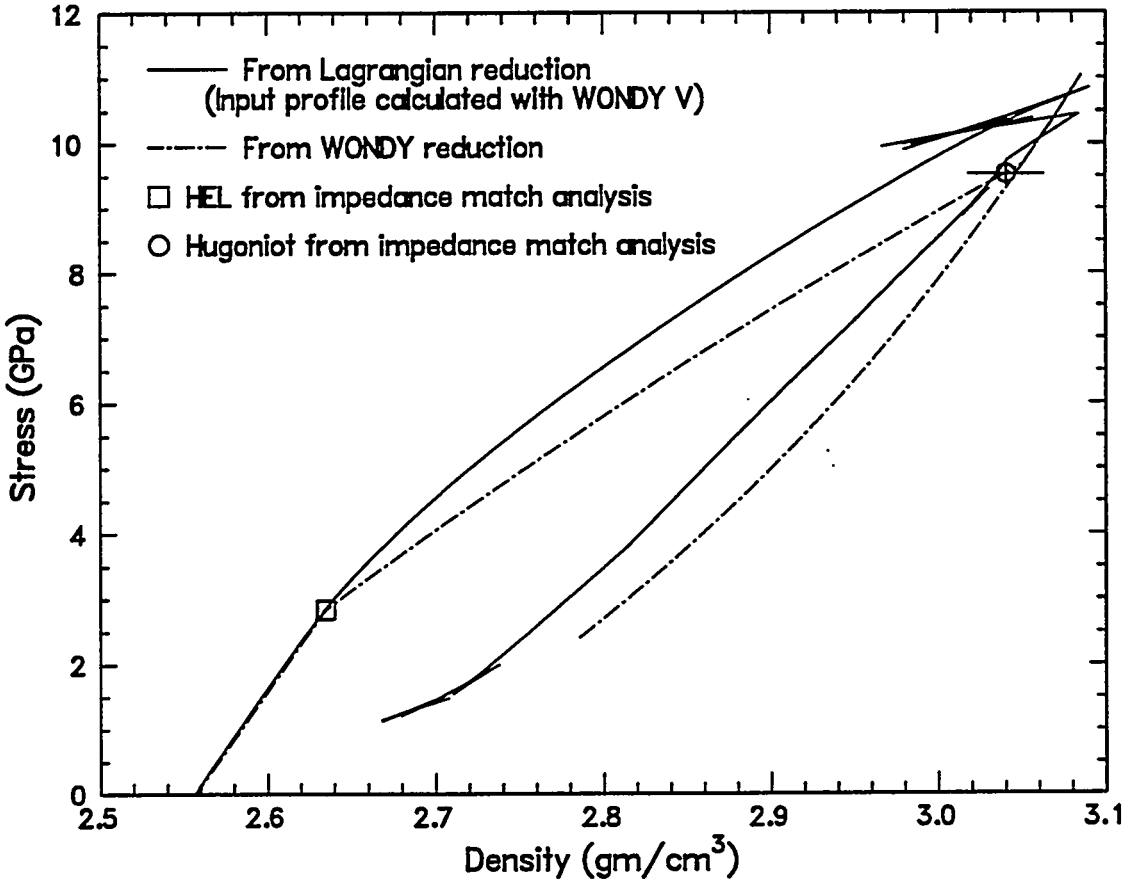

Figure 4-4. Comparison between two data reduction methods for test GR 4.

5.0 Conclusions

Three sets of rock samples have been subjected to planar impact to characterize loading, Hugoniot and release responses. A slate from Pennsylvania was tested over the stress range of 5 GPa to 140 GPa. Phyllite from the Lupin Mine (Canada) was tested over the 14 - 50 GPa stress region. Finally, granite from the SHIST test site (New Mexico) was tested over the 10 - 20 GPa stress region, including a transmitted-wave experiment at about 10 GPa. In 12 of the 13 tests, a reverse-ballistic configuration (optimized for Hugoniot and release measurements) was used, while the remaining test, conducted on the granite, provided a transmitted waveform from which precursor, Hugoniot and release properties were obtained. Velocity interferometry was used as the primary diagnostic throughout. The slate data showed an unexpected inflection downward in the Hugoniot at around 8 GPa. The slate and granite showed releases lying below the Hugoniot for lower stress levels (below ~60 GPa), while the slate releases were "normal" (above the Hugoniot) at higher stress levels. In addition, the granite releases were found to lie substantially below the Hugoniot in the 30 - 40 GPa region; this may be related to the quartz-stishovite transition (and analogous ^{IV}SI - ^{VI}SI transitions in the feldspars. The present results are generally consistent with earlier work.

References

Aidun, J. B and Y. M. Gupta, Shear wave measurements for improved characterization of shock-induced phase transformations in Carrera marble, *Geophys. Res. Lett., 16*, 191-194, 1989.

Anderson, W. W., Y. Zhao and T. J. Ahrens, Equation of state of clay, shale and slate, Defense Nuclear Agency Report DNA TR-95-32, 1995.

Barker, L. M. and R. E. Hollenbach, Shock-wave studies of PMMA, fused silica, and sapphire, *J. Appl. Phys., 41,* 4208-4226, 1970.

Barker, L. M. and R. E. Hollenbach, Laser interferometer for measuring high velocities of any reflecting surface, *J. Appl. Phys*, 43, 4669-4675, 1972.

Chhabildas, L. C., L. M. Barker, J. R. Asay and T. G. Trucano, Spall strength measurements on shock-loaded refractory metals, pp. 429-432 in *Shock Compression of Condensed Matter - 1989*, S. C. Schmidt, J. N. Johnson and L. W. Davison (eds.), Elsevier Science Publishers, 1990.

Furnish, M. D., L. C. Chhabildas, D. J. Steinberg and G. T. Gray III, Dynamic material properties of refractory materials: Molybdenum, pp. 229 - 240 in *High Strain Rate Behavior of Refractory Metals and Alloys*, R. Asfahani, E. Chen and A. Crowson (eds.), The Minerals, Metals and Materials Society, 1992.

Furnish, M. D., Measuring the dynamic compression and release behavior of rocks and grouts associated with HYDROPLUS, Sandia National Laboratories report SAND92-0984, 1993a.

Furnish, M. D., Recent advances in methods for measuring the dynamic response of geologic materials to 100 GPa, *Int. J. Impact Engng.*, **14**, 267-277, 1993b.

Furnish, M. D., Dynamic properties of Indiana, Fort Knox and Utah Test Range Limestones and Danby Marble over the stress range 1 to 20 GPa, Sandia National Laboratories report SAND92-0983, 1994.

Gaffney, E. S. and E. A. Smith, HYDROPLUS Experimental Study of Dry, Saturated, and Frozen Geological Materials, DNA Report DNA-TR-93-74, 1994

Grady, D. E. and M. D. Furnish, Shock- and Release-Wave Properties of MJ-2 Grout, Sandia report SAND88-1642, 1988.

Kipp, M. E. and R. J. Lawrence, WONDY V - A one-dimensional finite-difference wave propagation code, Sandia National Laboratories report SAND81-0930 (1982).

McQueen, R. G., S. P. Marsh, J. W. Taylor, J. N. Fritz and W. J. Carter, The equation of state of solids from shock wave studies, pp. 293 - 417 in R. Kinslow (ed.), *High Velocity Impact Phenomena*, Academic Press, 1970.

Marquardt, J. (Terra Tek Inc.), personal communication, Oct. 3, 1993.

Martin, W. (Terra Tek, Inc.), memorandum to A. Martinez, dated December 15, 1992.

Martin, W. (Terra Tek, Inc.), memorandum to A. Martinez, dated June 3, 1993(a).

Martin, W. (Terra Tek, Inc.). memorandum to A.Martinez, dated October 27, 1993(b).

Martin, J. W., C. W. Felice and J. Marquardt, Material property measurements on permafrost from the Lupin Mine, Canada, Terra Tek report TR93-31, 1992.

Meyers, S., (Lachel & Associates), memorandum to A. Martinez titled "Slate sampling trip report," dated December 18, 1992.

Schuler, K. W. and J. W. Nunziato, The dynamic behavior of polymethyl methacrylate, Rheol. Acta, 13, 265-273, 1975.

Davies, F. W. and Smith, E., High pressure equation of state investigation of rocks, Defense Nuclear Agency report, DNA-TR-94-1, 1994

Swegle, J. W. and D. E. Grady, Shock viscosity and the prediction of shock wave rise times, J. Appl. Phys., 58, 692, 1985.

USACDA/USOSIA (United States Arms Control and Disarmament Agency/United States On-Site Inspection Agency), Treaty between the USA and the USSR on the limitation of underground nuclear weapon tests and the Treaty between the USA and the USSR on underground nuclear explosions for peaceful purposes: texts of treaties and protocols, 1990.

Wise, J. L. and L. C. Chhabildas, Laser interferometer measurements of refractive index in shock-compressed materials, pp. 441-454 in Shock Waves in Condensed Matter, Y. M. Gupta (ed), Plenum, 1985.

Appendix A
Release Paths

Release paths for the tests discussed in this report are presented in a filtered form in this Appendix. Calculation of the pressure/volume release paths utilizes the Lagrangian wavecode WONDY V [Kipp and Lawrence, 1982], and is described in Appendix B. Conversion to particle velocity is done via a Riemann integration from the Hugoniot state [Furnish, 1993a,b]. Each path is represented by the first (Hugoniot), second and last points on the valid portion of the release, with the interval between the second and last points covered by five points equally spaced in pressure. Units are SI (Pa for pressure, m^3/kg for volume, kg/m^3 for density, m/s for particle velocity U_p, and J/kg for specific energy). Particle velocity is presented both incrementing upward and incrementing downward from the Hugoniot value to facilitate comparison with the results of other experiments; the true sense for the reverse-ballistic experiments is upward incrementation since the shock and the release are propagating in opposite directions.

Shot names and numbers are the same as those used in the text and tables. They are arranged alphabetically. The B_i parameters are listed consecutively; e.g. for Phy 1, we have $B_0 = 18.0 \times 10^{10}$ Pa, $B_1 = 0.85$, $B_2 = 0.07$and $B_3 = -0.05$.

Phy 1 B = 18.0, 0.85, 0.07, -0.05 No Cup

Pressure	Volume	Density	Up (+)	Energy	Up (-)
0.13858E+11	0.30410E-03	0.32884E+04	0.89100E+03	0.40341E+06	0.89100E+03
0.13838E+11	0.30414E-03	0.32880E+04	0.89189E+03	0.40286E+06	0.89011E+03
0.11987E+11	0.30806E-03	0.32461E+04	0.97708E+03	0.35371E+06	0.80492E+03
0.10137E+11	0.31248E-03	0.32002E+04	0.10676E+04	0.30745E+06	0.71444E+03
0.82862E+10	0.31756E-03	0.31490E+04	0.11644E+04	0.26344E+06	0.61757E+03
0.64356E+10	0.32349E-03	0.30912E+04	0.12692E+04	0.22253E+06	0.51278E+03
0.45850E+10	0.33055E-03	0.30253E+04	0.13834E+04	0.18631E+06	0.39858E+03
0.27344E+10	0.33912E-03	0.29488E+04	0.15093E+04	0.15746E+06	0.27270E+03

Phy 2 B = 54.0, 1.3, 0, -0.3 No Cup

Pressure	Volume	Density	Up (+)	Energy	Up (-)
0.34580E+11	0.24561E-03	0.40715E+04	0.20270E+04	0.19952E+07	0.20270E+04
0.34557E+11	0.24563E-03	0.40712E+04	0.20276E+04	0.19947E+07	0.20264E+04
0.31084E+11	0.24819E-03	0.40292E+04	0.21223E+04	0.19165E+07	0.19317E+04
0.27612E+11	0.25112E-03	0.39822E+04	0.22231E+04	0.18369E+07	0.18309E+04
0.24139E+11	0.25462E-03	0.39274E+04	0.23334E+04	0.17534E+07	0.17206E+04
0.20666E+11	0.25890E-03	0.38626E+04	0.24551E+04	0.16645E+07	0.15989E+04
0.17194E+11	0.26431E-03	0.37834E+04	0.25922E+04	0.15685E+07	0.14618E+04
0.13721E+11	0.27150E-03	0.36833E+04	0.27500E+04	0.14633E+07	0.13040E+04

Phy 3 B = 90.0, 3.0, 2.9, 0.8 Gap = 0.10 mm

Pressure	Volume	Density	Up (+)	Energy	Up (-)
0.48986E+11	0.21814E-03	0.45842E+04	0.26540E+04	0.34929E+07	0.26540E+04
0.48825E+11	0.21820E-03	0.45829E+04	0.26572E+04	0.34898E+07	0.26508E+04

Phy 3 B = 90.0, 3.0, 2.9, 0.8 Gap = 0.10 mm (Continued)

0.38902E+11	0.22442E-03	0.44560E+04	0.29042E+04	0.32322E+07	0.24038E+04
0.33941E+11	0.22978E-03	0.43521E+04	0.30670E+04	0.30447E+07	0.22410E+04
0.28980E+11	0.23815E-03	0.41990E+04	0.32703E+04	0.27901E+07	0.20377E+04
0.24018E+11	0.25213E-03	0.39662E+04	0.35329E+04	0.24314E+07	0.17751E+04
0.19057E+11	0.27636E-03	0.36184E+04	0.38785E+04	0.19250E+07	0.14295E+04

Gran 1 B = 13.0, 0.85, 0, -0.2

Pressure	Volume	Density	Up (+)	Energy	Up (-)
0.98299E+10	0.32196E-03	0.31060E+04	0.79800E+03	0.33151E+06	0.79800E+03
0.98117E+10	0.32201E-03	0.31055E+04	0.79899E+03	0.33099E+06	0.79701E+03
0.84039E+10	0.32647E-03	0.30631E+04	0.87821E+03	0.29124E+06	0.71779E+03
0.69961E+10	0.33158E-03	0.30158E+04	0.96300E+03	0.25295E+06	0.63300E+03
0.55883E+10	0.33753E-03	0.29627E+04	0.10545E+04	0.21701E+06	0.54150E+03
0.41806E+10	0.34453E-03	0.29026E+04	0.11537E+04	0.18452E+06	0.44227E+03
0.27728E+10	0.35284E-03	0.28342E+04	0.12618E+04	0.15724E+06	0.33417E+03
0.13650E+10	0.36266E-03	0.27574E+04	0.13794E+04	0.13869E+06	0.21660E+03

Gran 2 B = 17.0, 1.3, 0.3, -0.2

Pressure	Volume	Density	Up (+)	Energy	Up (-)
0.16534E+11	0.29647E-03	0.33730E+04	0.12390E+04	0.77963E+06	0.12390E+04
0.16521E+11	0.29650E-03	0.33727E+04	0.12396E+04	0.77913E+06	0.12384E+04
0.14616E+11	0.30121E-03	0.33200E+04	0.13343E+04	0.70697E+06	0.11437E+04
0.12711E+11	0.30676E-03	0.32600E+04	0.14370E+04	0.63260E+06	0.10410E+04
0.10806E+11	0.31340E-03	0.31908E+04	0.15495E+04	0.55703E+06	0.92845E+03
0.89007E+10	0.32150E-03	0.31104E+04	0.16737E+04	0.47997E+06	0.80431E+03
0.69957E+10	0.33154E-03	0.30163E+04	0.18119E+04	0.40323E+06	0.66614E+03
0.50906E+10	0.34410E-03	0.29062E+04	0.19665E+04	0.33037E+06	0.51150E+03

Gran 3 B = 18, 1.1, 0, -0.2

Pressure	Volume	Density	Up (+)	Energy	Up (-)
0.18186E+11	0.29409E-03	0.34003E+04	0.13250E+04	0.88896E+06	0.13250E+04
0.18178E+11	0.29411E-03	0.34001E+04	0.13254E+04	0.88864E+06	0.13246E+04
0.16073E+11	0.29898E-03	0.33447E+04	0.14266E+04	0.80645E+06	0.12234E+04
0.13969E+11	0.30460E-03	0.32829E+04	0.15355E+04	0.72350E+06	0.11145E+04
0.11864E+11	0.31124E-03	0.32129E+04	0.16536E+04	0.64080E+06	0.99642E+03
0.97593E+10	0.31927E-03	0.31322E+04	0.17835E+04	0.55724E+06	0.86652E+03
0.76547E+10	0.32930E-03	0.30368E+04	0.19287E+04	0.47335E+06	0.72131E+03
0.55500E+10	0.34232E-03	0.29212E+04	0.20941E+04	0.39044E+06	0.55590E+03

Gran 4 (SHIST) B = 17.5, 1, 0.5, 0.4

Pressure	Volume	Density	Up (+)	Energy	Up (-)
0.96725E+10	0.32779E-03	0.30507E+04	0.77600E+00	0.18898E+10	0.77600E+00
0.96668E+10	0.32781E-03	0.30506E+04	0.10786E+01	0.18898E+10	0.47340E+00
0.84591E+10	0.33143E-03	0.30172E+04	0.67226E+02	0.18898E+10	-0.65674E+02
0.72514E+10	0.33552E-03	0.29805E+04	0.13748E+03	0.18897E+10	-0.13593E+03
0.60437E+10	0.34017E-03	0.29397E+04	0.21243E+03	0.18897E+10	-0.21087E+03
0.48361E+10	0.34552E-03	0.28942E+04	0.29278E+03	0.18897E+10	-0.29123E+03
0.36284E+10	0.35172E-03	0.28431E+04	0.37932E+03	0.18896E+10	-0.37777E+03
0.24207E+10	0.35894E-03	0.27860E+04	0.47264E+03	0.18896E+10	-0.47109E+03

SLP1 B = 13.5, 0.85, 0, -0.2 Gap=0.043mm

Pressure	Volume	Density	Up (+)	Energy	Up (-)
0.52320E+10	0.33784E-03	0.29600E+04	0.37600E+03	0.70612E+05	0.37600E+03
0.51736E+10	0.33787E-03	0.29597E+04	0.37744E+03	0.70430E+05	0.37456E+03
0.43696E+10	0.34021E-03	0.29393E+04	0.42080E+03	0.59693E+05	0.33120E+03
0.35656E+10	0.34292E-03	0.29161E+04	0.46748E+03	0.49537E+05	0.28452E+03
0.27616E+10	0.34612E-03	0.28892E+04	0.51819E+03	0.39985E+05	0.23381E+03
0.19575E+10	0.34994E-03	0.28576E+04	0.57360E+03	0.31568E+05	0.17840E+03
0.11535E+10	0.35453E-03	0.28206E+04	0.63429E+03	0.25086E+05	0.11771E+03
0.34950E+09	0.35997E-03	0.27780E+04	0.70040E+03	0.21612E+05	0.51600E+02

SLP2 B = 18.0, 0.85, 0.07, -0.05 Gap=0.0321mm

Pressure	Volume	Density	Up (+)	Energy	Up (-)
0.86120E+10	0.31898E-03	0.31350E+04	0.62800E+03	0.19686E+06	0.62800E+03
0.84761E+10	0.31899E-03	0.31349E+04	0.62898E+03	0.19680E+06	0.62702E+03
0.71859E+10	0.32181E-03	0.31075E+04	0.68931E+03	0.17574E+06	0.56669E+03
0.58958E+10	0.32506E-03	0.30764E+04	0.75402E+03	0.15570E+06	0.50198E+03
0.46056E+10	0.32887E-03	0.30407E+04	0.82416E+03	0.13688E+06	0.43184E+03
0.33155E+10	0.33344E-03	0.29990E+04	0.90096E+03	0.12006E+06	0.35504E+03
0.20253E+10	0.33908E-03	0.29492E+04	0.98617E+03	0.10625E+06	0.26983E+03
0.73515E+09	0.34624E-03	0.28882E+04	0.10822E+04	0.97525E+05	0.17380E+03

SLP3 B = 22.0, 1.35, 0.6, -0.2 No gap

Pressure	Volume	Density	Up (+)	Energy	Up (-)
0.16274E+11	0.29976E-03	0.33360E+04	0.10290E+04	0.52948E+06	0.10290E+04
0.16129E+11	0.29994E-03	0.33340E+04	0.10341E+04	0.52659E+06	0.10239E+04
0.13951E+11	0.30393E-03	0.32902E+04	0.11274E+04	0.46837E+06	0.93063E+03
0.11772E+11	0.30876E-03	0.32387E+04	0.12299E+04	0.40918E+06	0.82814E+03
0.95939E+10	0.31461E-03	0.31786E+04	0.13427E+04	0.34990E+06	0.71532E+03
0.74155E+10	0.32160E-03	0.31095E+04	0.14660E+04	0.29433E+06	0.59200E+03
0.52372E+10	0.32967E-03	0.30334E+04	0.15986E+04	0.24854E+06	0.45940E+03
0.30588E+10	0.33842E-03	0.29549E+04	0.17367E+04	0.21764E+06	0.32130E+03

SLP4 B = 41.0, 2.0, 0.9, -0.2 Gap=0.06mm

Pressure	Volume	Density	Up (+)	Energy	Up (-)
0.26580E+11	0.26110E-03	0.38300E+04	0.16670E+04	0.13893E+07	0.16670E+04
0.26253E+11	0.26187E-03	0.38187E+04	0.16829E+04	0.13691E+07	0.16511E+04
0.23940E+11	0.26419E-03	0.37851E+04	0.17562E+04	0.13132E+07	0.15778E+04
0.21627E+11	0.26699E-03	0.37455E+04	0.18366E+04	0.12526E+07	0.14974E+04
0.19314E+11	0.27048E-03	0.36971E+04	0.19264E+04	0.11843E+07	0.14076E+04
0.17000E+11	0.27493E-03	0.36373E+04	0.20277E+04	0.11069E+07	0.13063E+04
0.14687E+11	0.28079E-03	0.35614E+04	0.21441E+04	0.10177E+07	0.11899E+04
0.12374E+11	0.28878E-03	0.34629E+04	0.22798E+04	0.91314E+06	0.10542E+04

SLP6 B =170.0, 1.35, 0.1, -0.3 No Gap

Pressure	Volume	Density	Up (+)	Energy	Up (-)
0.13971E+12	0.19547E-03	0.51160E+04	0.48720E+04	0.11868E+08	0.48720E+04
0.13890E+12	0.19564E-03	0.51113E+04	0.48840E+04	0.11843E+08	0.48600E+04
0.12721E+12	0.19837E-03	0.50416E+04	0.50624E+04	0.11517E+08	0.46816E+04
0.11552E+12	0.20141E-03	0.49655E+04	0.52508E+04	0.11193E+08	0.44932E+04

SLP6 B =170.0, 1.35, 0.1, -0.3 No Gap (Continued)

0.10382E+12	0.20487E-03	0.48814E+04	0.54520E+04	0.10857E+08	0.42920E+04
0.92131E+11	0.20895E-03	0.47861E+04	0.56702E+04	0.10503E+08	0.40738E+04
0.80438E+11	0.21383E-03	0.46771E+04	0.59088E+04	0.10127E+08	0.38352E+04
0.68746E+11	0.21970E-03	0.45516E+04	0.61707E+04	0.97195E+07	0.35733E+04

SLP7 B = 70.0, 1.5, 0.31, -0.2 Gap=0.012mm Lockstep

Pressure	Volume	Density	Up (+)	Energy	Up (-)
0.65713E+11	0.21744E-03	0.45990E+04	0.31220E+04	0.48735E+07	0.31220E+04
0.65175E+11	0.21747E-03	0.45983E+04	0.31261E+04	0.48714E+07	0.31179E+04
0.58990E+11	0.22101E-03	0.45249E+04	0.32740E+04	0.46624E+07	0.29700E+04
0.52805E+11	0.22513E-03	0.44420E+04	0.34336E+04	0.44488E+07	0.28104E+04
0.46620E+11	0.23008E-03	0.43465E+04	0.36084E+04	0.42214E+07	0.26356E+04
0.40434E+11	0.23610E-03	0.42356E+04	0.38013E+04	0.39775E+07	0.24427E+04
0.34249E+11	0.24371E-03	0.41033E+04	0.40181E+04	0.37119E+07	0.22259E+04
0.28064E+11	0.25365E-03	0.39425E+04	0.42658E+04	0.34176E+07	0.19782E+04

Appendix B
Model Wave Profiles Fit to Experiments

This Appendix shows the waveforms generated by the wavecode WONDY V [Kipp and Lawrence, 1982] which best fit the experimental waveforms. The loading equation-of-state for the sample is modeled by a single-shock Mie-Grüneisen behavior. Precursors (elastic or due to phase transitions) may also be included, but were not for the present tests. The unloading behavior is governed by a stress-dependent longitudinal modulus (Eq. B.1).

$$\frac{\delta P}{\delta V} = \frac{-B_0}{V}\left(1 + B_1\chi + B_2\chi^2 + B_3\chi^3\right), \text{ where } \chi \equiv \frac{P}{P_{Hug}} - 1 \qquad \text{(Eq. B.1)}$$

In addition, if a pullback signature is observed in the waveform after the initial plateau, a gap between the sample and the cup is assumed. For these cases, a gap of some width is included in the model, with the width chosen to give a fit to the observed signature. This does not apply for forward-ballistic tests or reverse-ballistic tests with no cup to contain the sample.

Hence the adjustable parameters are the four B_i and the gap width (where applicable).

The following figures each present an experimental waveform (plotted as small solid squares) overlain by a model waveform calculated by WONDY V. The four B_i and the gap width used in the model (where applicable) are noted. B_0 is in units of 10 GPa; all other B_i are unitless.

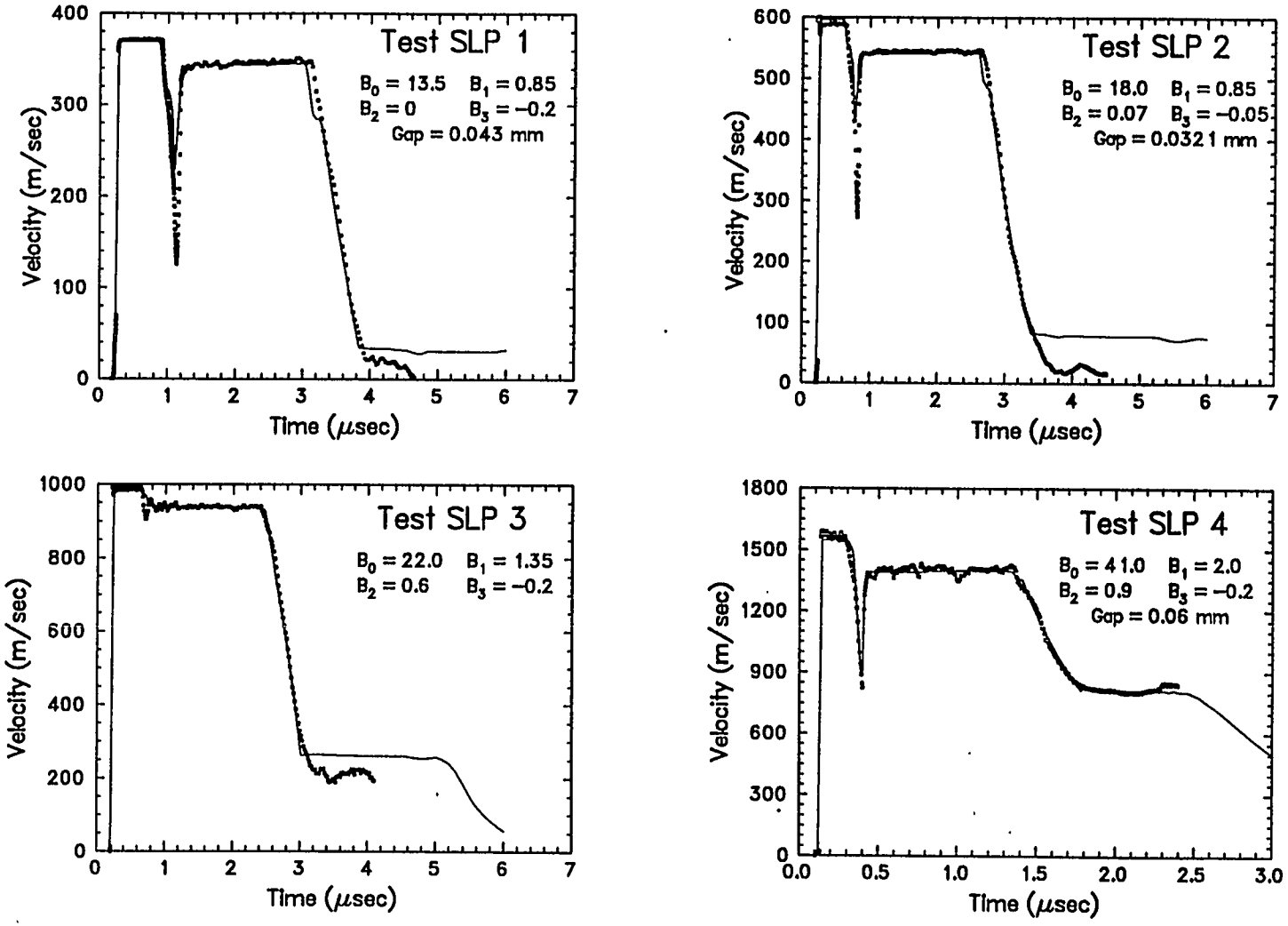

Figure B-1. WONDY V fits to Tests SLP1 - SLP4.

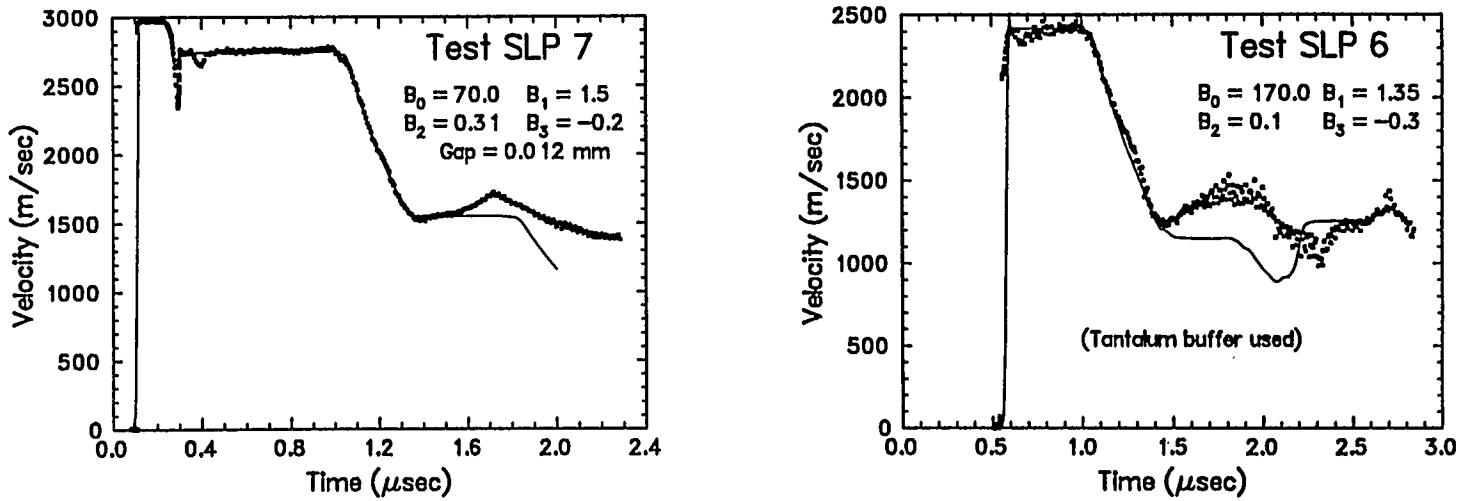

Figure B-2. WONDY V fits to Tests SLP6 - SLP7.

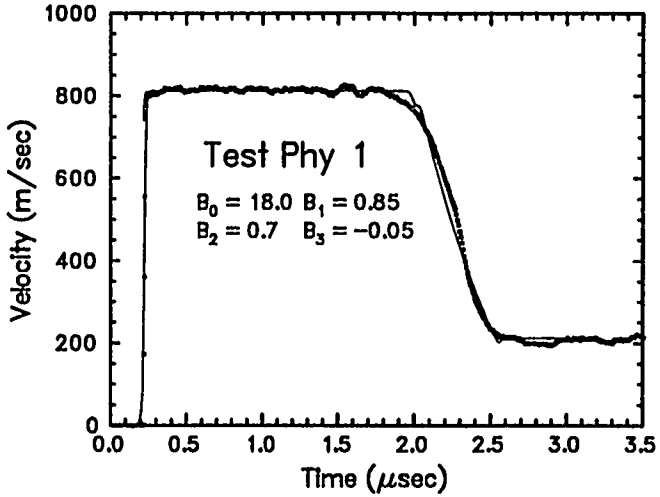

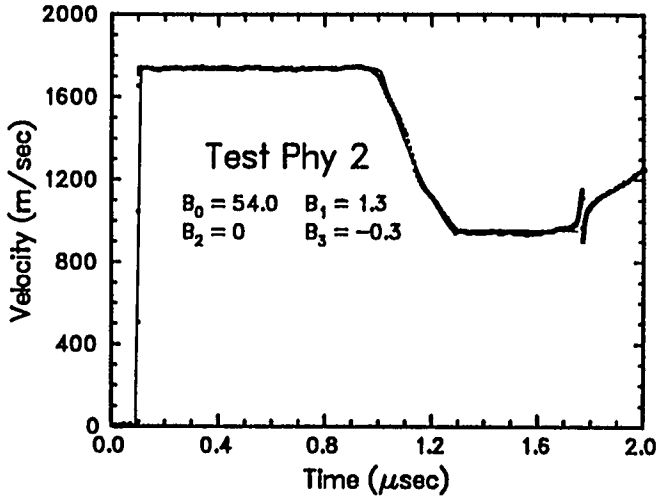

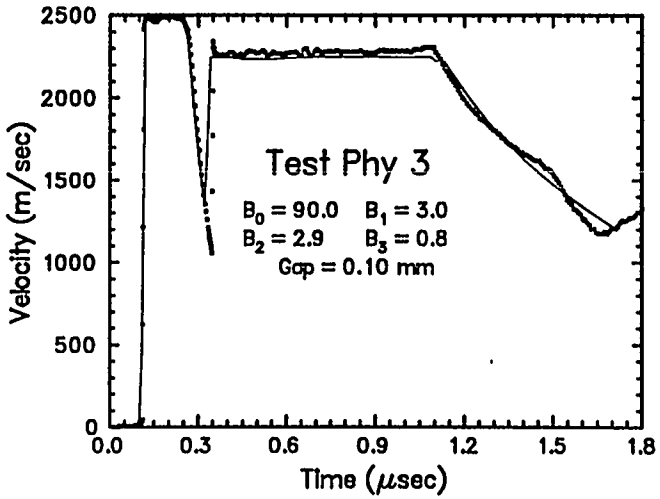

Figure B-3. WONDY V fits to Tests Phy 1 - Phy 3.

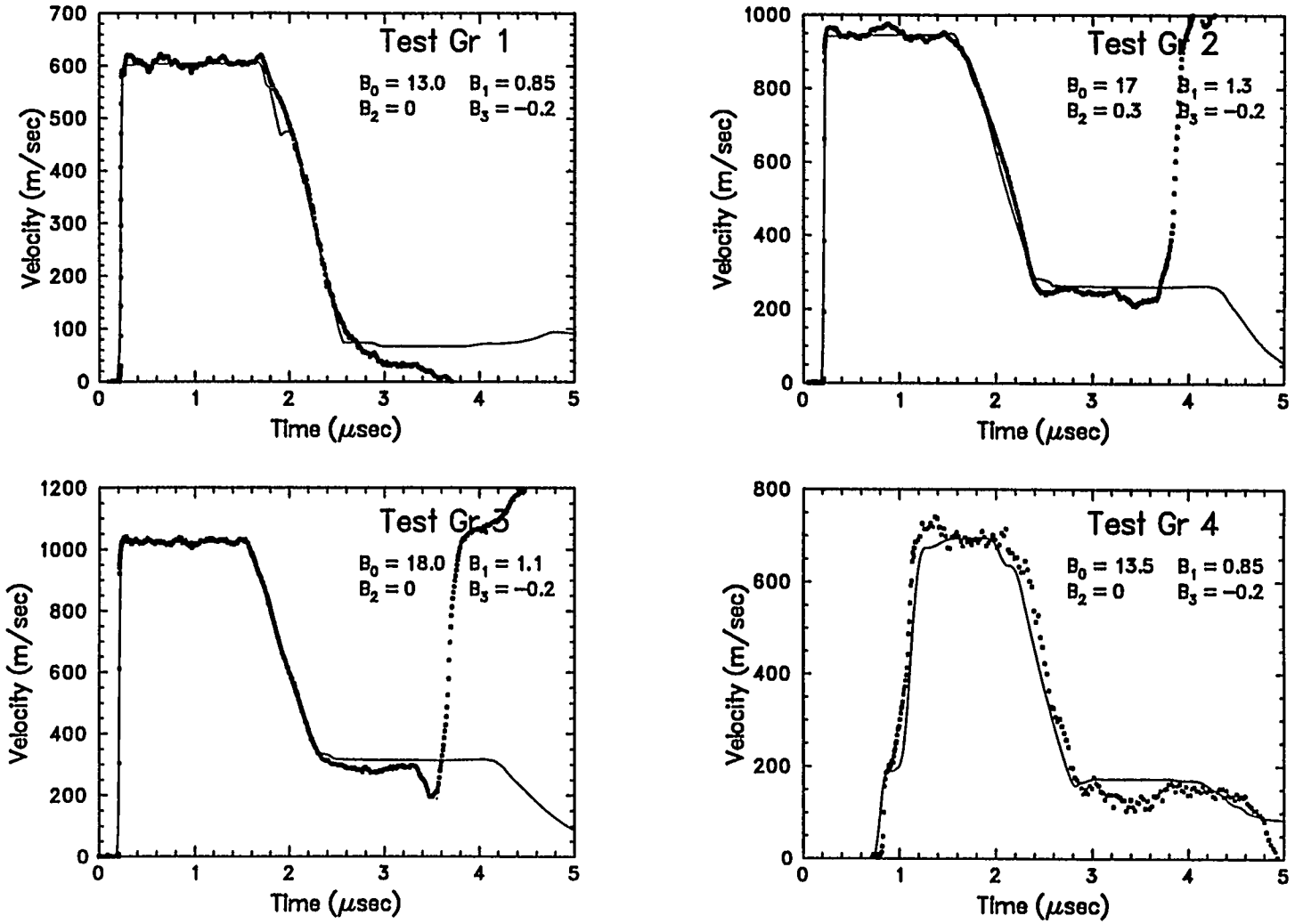

Figure B-4. WONDY V fits to Tests GR 1 - GR 4.

This page intentionally left blank

Distribution

External Distribution:

Titan Research and Technology
9410 Topanga Canyon Blvd #104
Chatsworth, CA 91311-5758
Attn:
Anne Cooper
Sheldon Schuster

CEWES-SD
Waterways Experiment Station
3909 Halls Ferry Road
Vicksburg, MS 39180
Attn:
John Boa
Tony Bombich

DNA Nevada Operations Office
P.O. Box 98539
Las Vegas, NV 89193-8539
Attn:
Barbara Harris-West

FCDNA/FCTTS
1680 Texas St SE
Kirtland AFB, NM 87117
Attn:
George Baladi, FCTTS
Mike O'Brien, FCTO
George Lu, FCTI
Audrey Martinez, FCTTS
Eric Rinehart, FCTTS
Bob Reinke, FCTTS
Byron Rystvit, FCTTS

HQ/DNA
6801 Telegraph Road
Alexandria, VA 22310-3398
Attn:
Don Linger, DFTD
Fran Rensvold, DFTD
SSTS (2)

Ktech Corp
901 Pennsylvania Ave NE
Albuquerque NM 87110
Attn:
Frank Davies
Eric Smith

Lawrence Livermore National Laboratory
P.O. Box 808
Livermore, CA 94550
Attn:
Armand Attia, Mail Stop L-200
Dave Erskine, Mail Stop L-417
Lewis Glenn, Mail Stop L-200
Bill Moran, Mail Stop L-200
Kurt Sinz, Mail Stop L-200

Los Alamos National Laboratory
Los Alamos. NM 87545
Attn:
John Boettger, T-1, M/S B221
Arthur Cox, T-6 M/S B268
Thomas Dey, EES-5 M/S F665
James D. Johnson, T-1 M/S B221
James N. Johnson, T-1 M/S B221

Logicon R&D Associates
P.O. Box 9377
Albuquerque, NM 87119
Attn:
Larry Germain
Barbara Killian

SAIC/Pacifica Technology
10260 Campus Point Drive, MS 62
San Diego, CA 92121
Attn:
Martin Fogel
Dan Patch
Mike McKay
Jack Klump

S-Cubed, A Division of Maxwell Laboratories, Inc.
3398 Carmel Mountain Road
San Diego, CA 92121
Attn:
Jim Baker
Steve Peyton

S-Cubed, A Division of Maxwell Laboratories, Inc.
P.O. Box 1620
San Diego, CA 92038-1610
Attn:
Phil Coleman
Norton Rimer

Robert Bass
4505 Durango Ct. NE
Albuquerque, NM 87109

SRI International
333 Ravenswood Ave.
Menlo Park, CA 94025
Attn:
Don Curran
Paul deCarli

Thomas J. Ahrens
Seismological Laboratory
Division of Geological and Planetary Sciences
California Institute of Technology
Pasadena, CA 91125

Tom Duffy
Carnegie Institution of Washington
Geophysical Laboratory
5251 Broad Brach Road, NW
Washington, D. C. 20015-1305

Conrad Felice
Mission Research Corporation
9 Exchange Place
Suite 900
Salt Lake City, UT 84111

Paul Fisher
Springfield Research Facility
P.O. Box 1220
Springfield, VA 22151

Edward S. Gaffney
GRE Corp
2921 Carlisle Blvd NE
P.O. Box 30863
Albuquerque NM 87190-0863

Yogi. M.Gupta
Dept. of Physics
Shock Dynamics Laboratory
Washington State University
Pullman, WA 99124-2814

Skip Knowles
JAYCOR
1608 Spring Hill Road
Vienna, VA 22182-2270

Wesley Martin
Terra Tek
420 Wakara Way
Salt Lake City, Utah 84108

Frank McMullen
Tech Reps
5000 Marble Ave NE
Albuquerque NM 87110-6390

John L. Remo
Quantametrics, Inc.
#1 Brackenwood Path
Head of the Harbor
St. James, NY 11780

Ken Sites
SAIC
P.O. Box 19057
Las Vegas, NV 89119

Sandia Internal Distribution:

MS 0321 1400 E. H. Barsis
MS 1111 1402 R. J. Pryor
MS 0318 1403 G. S. Davidson
MS 1110 1404 J. A. Ang
MS 1111 1421 S. Dosanjh
MS 1110 1422 R. C. Allen
MS 1110 1423 Manager
MS 1109 1424 A. L. Hale
MS 0441 1425 P. L. Stanton
MS 0819 1431 J. M. McGlaun
MS 0820 1432 A. Farnsworth
MS 0820 1432 G. I. Kerley
MS 0820 1432 M. E. Kipp
MS 0820 1432 F. R. Norwood
MS 0820 1432 P. Yarrington
MS 0821 1433 L. C. Chhabildas
MS 0821 1433 D. Crawford
MS 0821 1433 M. D. Furnish (20)
MS 0821 1433 D. E. Grady
MS 0439 1434 D. R. Martinez
MS 0437 1562 E. P. Chen
MS 1454 2654 L. J. Weirick
MS 0427 5101 R. McIntosh
MS 0458 5602 J. R. Asay
MS 1033 6111 J. L. Wise
MS 0751 6117 W. R. Wawersik
MS 1345 6347 L. Hill
MS0100 7613-2 Document processing
for DOE-OSTI (2)
MS 9018 8523-2 Central Technical Files
MS 1160 9312 T. K. Bergstresser
MS 1160 9312 C. Smith
MS 0312 9814 M. J. Forrestal
MS 0619 12615 Print Media
MS 0899 13414 Technical Library (5)